

**Applied Meteorology Unit
(AMU)**

**Quarterly Report
Fourth Quarter FY-99**

Contract NAS10-96018

31 October 1999

**ENSCO, Inc.
1980 N. Atlantic Ave., Suite 230
Cocoa Beach, FL 32931
(407) 853-8202 (AMU)
(407) 783-9735**

Distribution:

NASA HQ/Q/F. Gregory
NASA HQ/AS/F. Cordova
NASA KSC/PH/D. King
NASA KSC/PH/Launch Director
NASA KSC/AA-C/L. Shriver
NASA KSC/AA/R. Bridges
NASA KSC/MK/D. McMonagle
NASA KSC/PZ-H/M. Wetmore
NASA KSC/PZ-H-C/D. Frostrum
NASA KSC/AA-C-1/J. Madura
NASA KSC/AA-C-1/F. Merceret
NASA KSC/BL/J. Zysko
NASA KSC/MM-E/G. Allen
NASA KSC/MM-G/O. Toledo
NASA JSC/MA/T. Holloway
NASA JSC/ZS8/F. Brody
NASA JSC/MS4/J. Richart
NASA JSC/MS4/R. Adams
NASA JSC/DA8/W. Hale
NASA MSFC/ED44/D. Johnson
NASA MSFC/ED44/B. Roberts
NASA MSFC/ED44/B. James
NASA MSFC/SA0-1/A. McCool
NASA MSFC/EL23/S. Pearson
45 WS/CC/D. Urbanski
45 WS/DOR/W. Tasso
45 WS/SY/D. Harms
45 WS/SYA/B. Boyd
45 RANS/CC/S. Liburdi
45 OG/CC/P. Benjamin
45 LG/CC/B. Evans
45 LG/LGQ/R. Fore
CSR 1300/M. Maier
CSR 4140/H. Herring
45 SW/SESL/D. Berlinrut
SMC/CWP/Coolidge
SMC/CWP/J. Rodgers
SMC/CWP/T. Knox
SMC/CWP/R. Bailey
SMC/CWP (PRC)/P. Conant
Hq AFSPC/DORW/S. Carr
Hq AFWA/CC/C. French
Hq AFWA/DNX/R. Lefevre
Hq AFWA/DN/N. Feldman
Hq USAF/XOW/F. Lewis
Hq AFRL/XPPR/B. Bauman
Office of the Federal Coordinator for Meteorological Services and Supporting Research
SMC/SDEW/B. Hickel
NOAA "W/OM"/L. Uccellini
NOAA/OAR/SSMC-I/J. Golden
NOAA/ARL/J. McQueen
NOAA Office of Military Affairs/L. Freeman

University of Berkeley – ROTC/T. Adang
NWS Melbourne/B. Hagemeyer
NWS Southern Region HQ/“W/SRH”/X. W. Proenza
NWS Southern Region HQ/“W/SR3”/D. Smith
NSSL/D. Forsyth
NWS/“W/OSD5”/B. Saffle
FSU Department of Meteorology/P. Ray
NCAR/J. Wilson
NCAR/Y. H. Kuo
30 WS/CC/C. Davenport
30 WS/SYR/S. Sambol
30 SW/XP/R. Miller
NOAA/ERL/FSL/J. McGinley
SMC/CLNER/B. Kempf
Aerospace Corp./B. Lundblad
Tetrattech/NUS Corp./H. Firstenberg
ENSCO Contracts/F. Warchal

Executive Summary

This report summarizes the Applied Meteorology Unit (AMU) activities for the fourth quarter of Fiscal Year (FY) 99 (July - September 1999). A detailed project schedule is included in the Appendix.

Ms. Lambert continued work on the Short Range Statistical Forecast Guidance task by performing an exploratory data analysis on the National Weather Service Melbourne (NWS MLB) hourly surface observations of ceiling and visibility to determine any dependence of different flight category occurrences on season or time of day. The lower flight categories seemed to occur predominately in the cool season (October through March) and during the morning hours. The data sets were then stratified into warm and cool seasons and new forecast equations were derived. Further analysis of the individual forecasts in event and non-event cases showed that the equations had little skill in being able to forecast occurrences flight categories due to low ceilings or visibilities. The AMU recommends that these equations not be used in operations.

Dr. Riewe began working on the portion of the Short Range Statistical Forecast Guidance task that requires development of wind speed and direction forecasts at the launch pad towers and within the wind tower network. He began by developing quality control (QC) algorithms to flag erroneous values in the data sets. Five algorithms in all were developed. These routines check the data for unrealistic values, vertical and temporal consistency, deviation from a mean value, and limits on the peak-to-average wind speed ratio.

Dr. Manobianco completed revisions on the final report describing the evaluation of data collected from a sodar located on the Kennedy Space Center (KSC). Data from tower 313 in the wind tower network were used in comparison with the sodar to evaluate its accuracy and reliability. The root mean square (RMS) differences in wind speed and wind direction from sodar wind solution B at KSC range from 0.65 m s^{-1} – 2.04 m s^{-1} and 4.5 – 32.3° , respectively. Note that these RMS differences are not bias-corrected. The vendor claims that the accuracy of the wind measurements from the sodar is better than 0.5 m s^{-1} in speed and 10° in direction (Sensor Technology Research, Inc. NASA SBIR phase II final report briefing). The results of the evaluation described here suggest that such accuracy may be attainable though the data available for this comparison made it impossible to confirm the vendor's claims because the reference tower was 3.5 km from the sodar.

Mr. Wheeler, Mr. Dianic, and Mr. Case continued work on the evaluation of the Regional Atmospheric Modeling System (RAMS) in the Eastern Range Dispersion Assessment System (ERDAS). Mr. Case compiled the preliminary results for warm season data from May through August 1999 for both the objective and subjective components of the task. The objective evaluation results indicate that wind speeds were slightly too strong on average following the sea-breeze passage. Forecast wind direction was virtually unbiased and non-systematic errors composed most of the total model error. The most notable systematic error introduced by the model is a near-surface cool temperature bias that occurred during the daylight hours. The subjective evaluation showed that ERDAS RAMS did an excellent job in forecasting the onset and movement of the Florida East Coast Sea Breeze (ECSB). The timing errors associated with the forecast ECSB at selected towers in the Kennedy Space Center/Cape Canaveral Air Station (KSC/CCAS) network were on the order of 1 h which is the temporal resolution of the data used for the evaluation.

Mr. Case completed the first draft of the final report describing the results from the Local Data Integration System (LDIS) task extension (Phase II). The LDIS Phase II final report describes the methodology in archiving a real-time data set, the modified configuration for the simulated real-time LDIS, sample case studies, and the sensitivities and deficiencies encountered. Also, hardware and software recommendations are provided for customer implementation of a real-time LDIS.

SPECIAL NOTICE TO READERS

AMU Quarterly Reports are now published on the Wide World Web (WWW). The Universal Resource Locator for the AMU Home Page is:

<http://technology.ksc.nasa.gov/WWWaccess/AMU/home.html>

The AMU Home Page can also be accessed via links from the NASA KSC Internal Home Page alphabetical index. The AMU link is "CCAS Applied Meteorology Unit".

If anyone on the current distribution would like to be removed and instead rely on the WWW for information regarding the AMU's progress and accomplishments, please respond to Frank Merceret (407-867-0818, francis.merceret-1@ksc.nasa.gov) or Winifred Lambert (407-853-8130, lambert.winifred@ensco.com).

1. BACKGROUND

The AMU has been in operation since September 1991. Tasking is reviewed annually with reviews at least semi-annually. The progress being made in each task is discussed in Section 2 with the primary AMU point of contact reflected on each task and/or subtask.

2. AMU ACCOMPLISHMENTS DURING THE PAST QUARTER

2.1 TASK 001 AMU OPERATIONS

Mr. Case visited the Spaceflight Meteorology Group (SMG) at Johnson Space Center (JSC) from 24-29 July to observe weather operations in support of the STS-93 landing. Mr. Richard Lafosse helped arrange the visit. Mr. Frank Brody, Mr. Tim Garner, and Mr. Tim Oram explained the motivation and methodology behind many of the operational support procedures during the visit. Mr. Mark Keehn provided Mr. Case with a tour of the facilities including the past and present Mission Control Centers. Mr. Case also met with Mr. Brody to discuss aspects of SMG operations including organization, responsibilities, and issues associated with forecasting and evaluating Shuttle flight rules at time ranges from 0 to 5 days.

While at JSC, Mr. Case presented the results of the Local Data Integration System (LDIS) task extension to several SMG staff members. The presentation was well received by SMG and will help to provide a preview of the types of real-time products that will be available once LDIS is installed locally at SMG. Discussions regarding the type of system hardware to be installed for a real-time LDIS occurred during the course of the presentation. Overall, the visit helped maintain the two-way flow of information between SMG and the AMU by face-to-face discussions of work that is usually described only through written reports.

In September, the AMU received several pieces of new equipment, which were installed by Mr. Wheeler. An IBM model 7043-260 RISC 6000 dual processor workstation with two external hard drives was added to the AMU Local Area Network (LAN) and configured. The AMU also received a Tektronix model 740 color laser printer. It was added to the AMU LAN and all individual workstations were configured to access the printer. The AMU also received several upgrades to existing software and a digital camera.

2.2 TASK 003 SHORT-TERM FORECAST IMPROVEMENT

SUBTASK 3 STATISTICAL SHORT-RANGE FORECAST TOOLS (MS. LAMBERT)

Ceiling and Visibility

In the previous Quarterly Report (FY99 Q3) the results of the development and testing of the observations-based equations (Vislocky and Fritsch, 1997) indicated poor performance for the technique. It was decided at that time that other steps would be taken in order to improve the performance of these equations. The first step would be to perform an exploratory data analysis (EDA) to determine any seasonal and/or time-of-day dependence on the

occurrence of the ceiling and visibility categories. The data could then be stratified into the appropriate time periods. Results from the EDA are shown in Figures 1 –5.

Figure 1 shows the number of occurrences of each category by month over the 25-year period of record (POR). The three categories of Low Instrument Flight Rules (LIFR), Instrument Flight Rules (IFR), and Marginal Visual Flight Rules (MVFR) due to ceiling are shown. The occurrences of Visual Flight Rules (VFR) occurrences are not shown because the numbers are very large (> 100,000). Including them on the graph would not allow the plots of the lower flight categories to be resolved. Overall, there is an obvious seasonal change in the number of occurrences of these three categories. The curves start at a peak in January, then gradually decrease through March. They become generally flat from April through September, then increase through October and November to the peak in December.

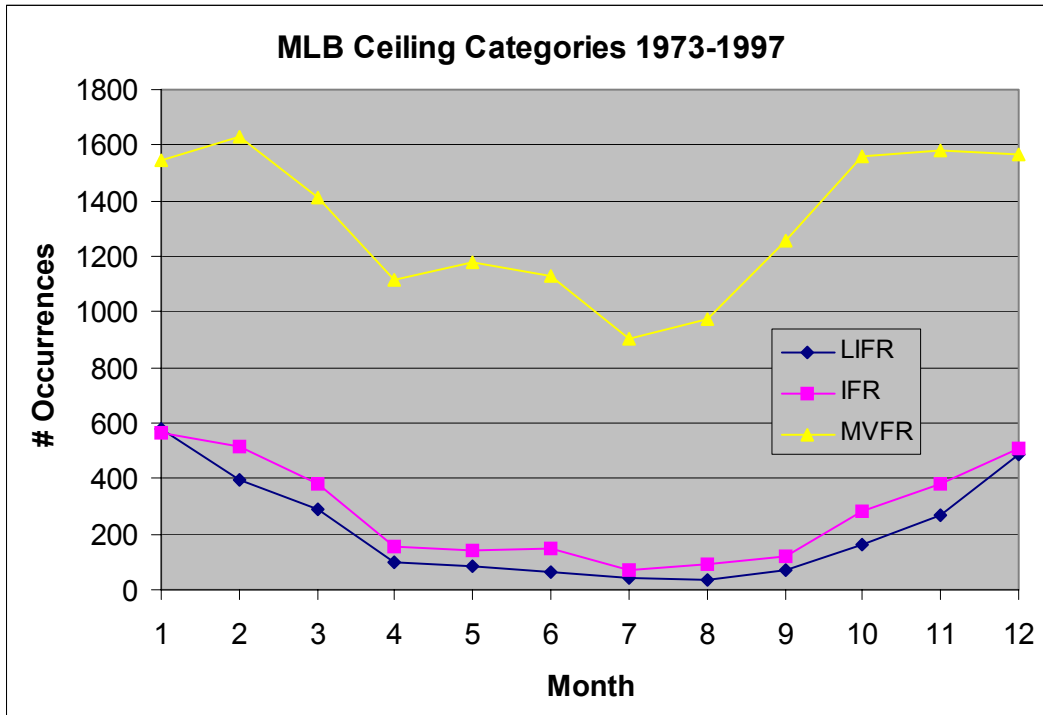


Figure 1. Graph showing number of occurrences by month of each of the flight categories of LIFR, IFR, and MVFR due to ceiling as observed at NWS MLB from 1973 to 1997.

Figure 2 is similar to Figure 1, except the categories are caused by visibility. Again, there is a seasonal change in the number of occurrences of these three categories. The curves in the two figures are similar, except that there is an increase in the number of MVFR occurrences in May, June, and July. Based on the curves in Figures 1 and 2, the data set was stratified into a warm season and a cool season. The warm season is defined as the months April through September, and the cool season is from October through March.

Data from the stratified data sets were then examined by time of day. Figure 3 shows the curves of the number of occurrences by hour for each category due to ceiling in the cool season. There is a gradual rise in the LIFR curve from 0500 UTC to the peak at 1300 UTC, then a sharp decrease to 1700 UTC where the curve flattens out. The peak in IFR follows the LIFR peak at 1500 UTC. The MVFR curve is relatively flat up to 1400 UTC, increasing sharply to the peak at 1800 UTC, then decreasing again. The general pattern shows that each higher ceiling category peaks shortly after the category below it.

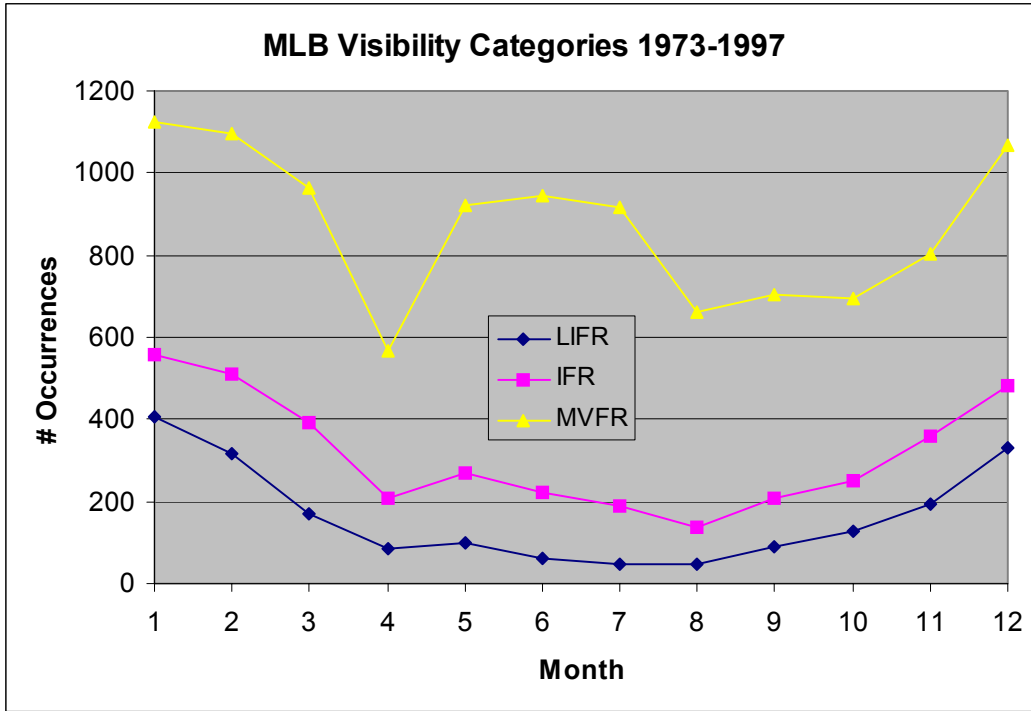


Figure 2. Graph showing number of occurrences by month of each of the flight categories of LIFR, IFR, and MVFR due to visibility as observed at NWS MLB from 1973 to 1997.

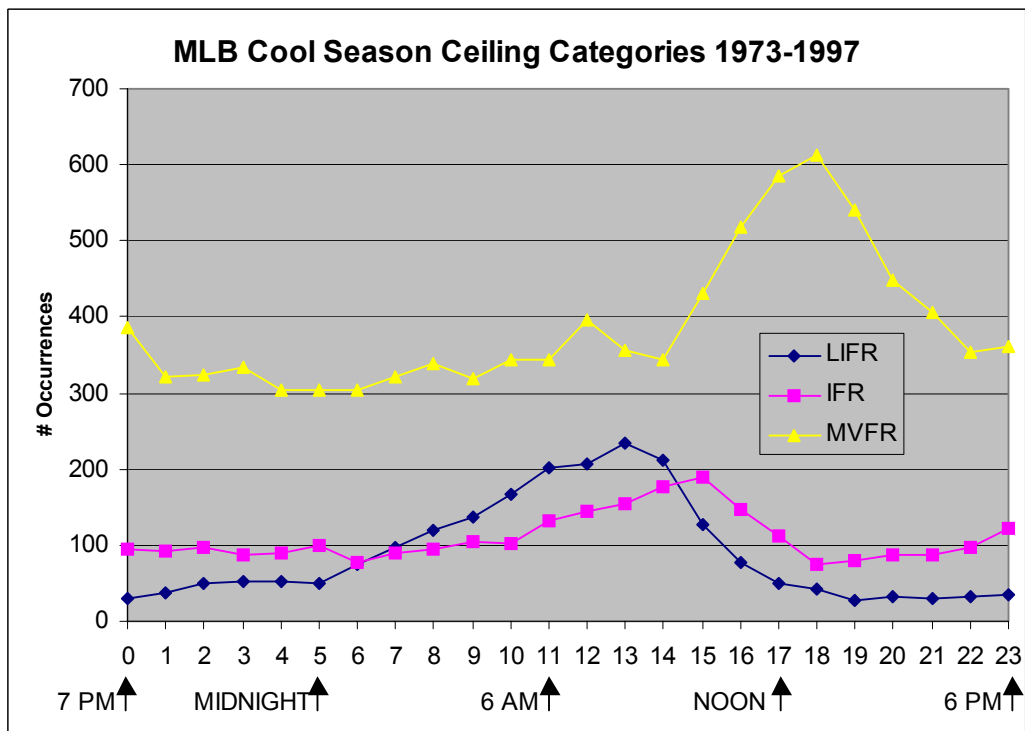


Figure 3. Graph showing number of occurrences by time of day of each of the flight categories of LIFR, IFR, and MVFR due to ceiling as observed at NWS MLB from 1973 to 1997.

Figure 4 shows the curves of the number of occurrences by hour for each category due to visibility in the cool season. All three curves show the same trend: sharp peaks at 1200 UTC with relatively gradual increases from ~0500 UTC and sharp decreases to 1500 UTC. Figures 3 and 4 show that most occurrences of the lower flight categories occur in the early to mid-morning hours.

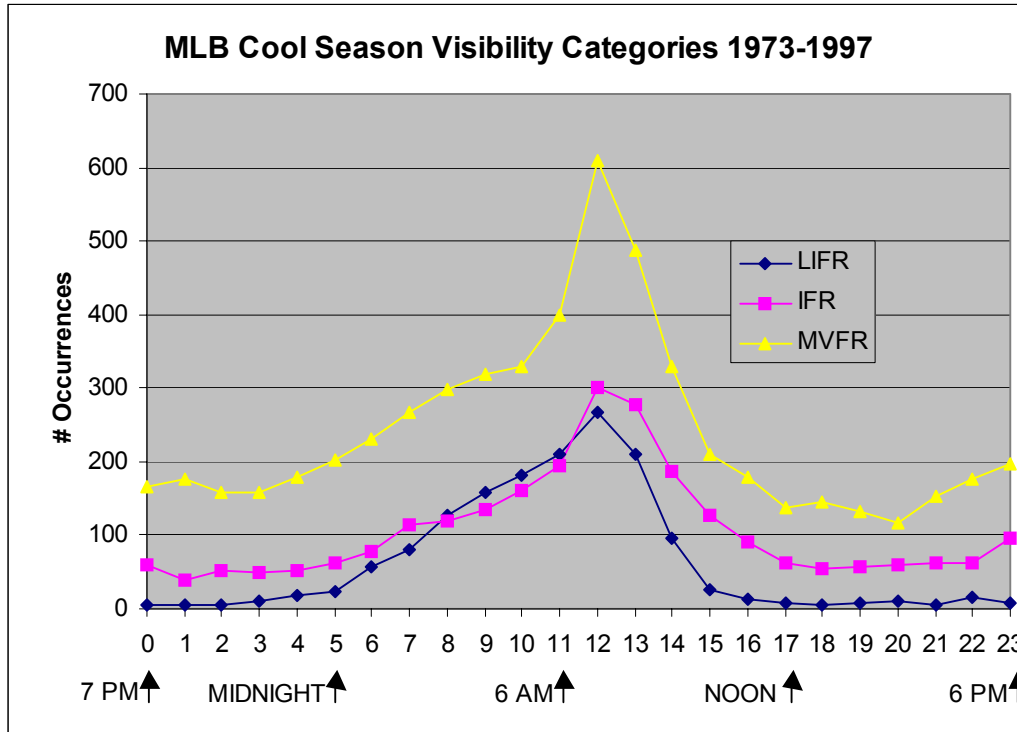


Figure 4. Graph showing number of occurrences by time of day of each of the flight categories of LIFR, IFR, and MVFR due to visibility as observed at NWS MLB from 1973 to 1997.

The progression of the peak with time seen in Figure 3 prompted an investigation to determine if there was a pattern in the change of flight category with time. Figure 5 contains four histograms that count the number of times a particular flight category remained the same or changed from 1200 – 1300 UTC. If the category changed, the number of times it changed to another particular category was counted.

The upper left panel shows the numbers for a 1200 UTC observation of LIFR conditions due to ceiling (directions on how to interpret the histogram are given in the figure caption). The column that counts the number of occurrences when the observation is LIFR at 1300 UTC is the largest at 163 indicating that persistence may be a good 1-hour forecast for LIFR at 1300 UTC. The same is true for IFR in the lower left panel with 84 occurrences of IFR remaining the same after an hour. However, if the other columns (CI2L, CI2M, and CI2V) were added together, they would total 106 which is more than the IFR occurrences. Thus it is more likely that the observation at 1300 UTC would be something other than IFR. In the upper right panel for 1200 UTC MVFR occurrences, the column for a change to VFR is almost equal to the column in which MVFR was observed at 1300 UTC. Similar to IFR, the conditions at 1300 UTC are as likely to be different as they are the same at 1200 UTC. The lower right panel shows that a persistence forecast for VFR is likely to be accurate. Overall, no pattern in the change of a category with time was evident.

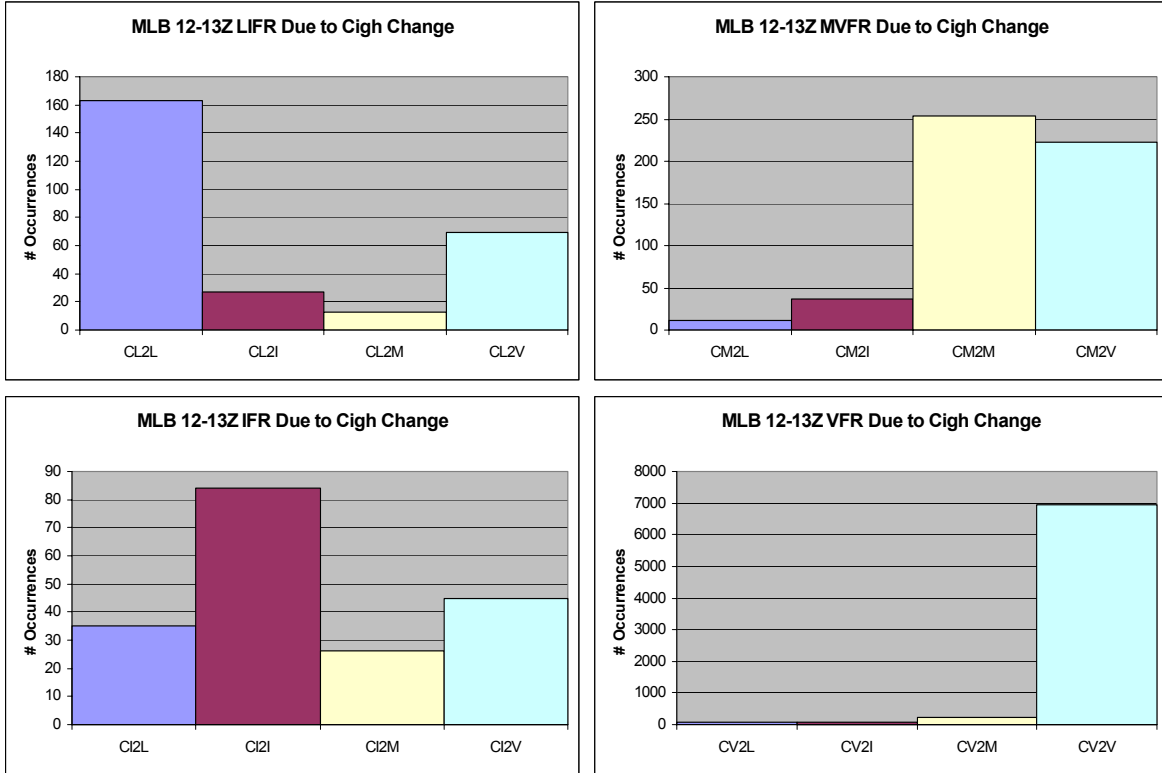


Figure 5. Histograms showing the number of times a particular flight category (due to ceiling) either remained the same or changed to another category from 1200 – 1300 UTC. In the labels underneath the columns, the ‘C’ denotes that the category was due to ceiling, the ‘L’ represents LIFR, the ‘I’ represents IFR, the ‘M’ represents MVFR, and the ‘V’ represents VFR. As an example, the label ‘CL2I’ can be read as ‘LIFR to IFR, both due to ceiling’.

Based on the seasonal stratification, new equations were tested and developed using the cool season data since most of the observations of the three lower flight categories occurred during those months. The examination of the number of occurrences by time of day confirmed the choice of using 1200 and 1300 UTC as the initialization and forecast times, respectively. Most occurrences of the lower three flight categories were observed in the morning hours.

In all, four forecast equation sets, or modes, were developed and tested. Two modes used 1200 UTC as the initial time, the other two used 1100 UTC, and all forecasts were valid for 1300 UTC. The 1100 UTC initial time was requested by NWS MLB, as they must issue forecasts at this time that are valid for 1300 UTC. The first 1200 UTC forecast used the data from all months in the equation development, and the second only used cool season data from October through March. The first 1100 UTC forecast used the cool season data set for equation development and the second used data from December and January. Stratification of the data set into two months from 1200 UTC caused a large drop in the number of events occurring in each category. Therefore, the relationships from 1000 – 1200 UTC and 1200 – 1400 UTC were considered in the development of the 1100 – 1300 UTC forecast equation. This increased the number of events in the data set to similar numbers found in the cool season data set.

The Brier Score (B), defined as the average of the squared differences between the observations and the forecasts, was then calculated for each forecast in all four modes using the equation

$$B = \frac{1}{n} \sum_{i=1}^n (f_i - o_i)^2,$$

where n is the number of observation/forecast pairs in the data set, f is the 1300 UTC probability forecast (0 to 1,

inclusive), and o is the 1300 UTC observation (0 or 1). The Brier Score was then used to calculate the percent improvement given by the observations-based forecast over the persistence and persistence climatology forecasts. The percent improvement is also known as the Skill Score (S) and is given by the equation

$$S = \frac{(B - B_r)}{(B_0 - B_r)} \times 100,$$

where B is the observations-based forecast Brier Score, B_r is the Brier Score of the reference forecast (persistence or persistence climatology), and B_0 is the Brier Score for a perfect forecast. Since the Brier Score is calculated using the difference between the forecast and the observation, B_0 is 0. The quantity is multiplied by 100 to yield a percent value.

Table 1 shows the skill scores from the comparison of all four modes of obs-based equations with their corresponding benchmarks using the independent data set. A definite improvement in skill of the 1200 – 1300 UTC obs-based forecast over the benchmarks of persistence climatology and persistence occurred when the cool-season data set was used. Further improvement in skill was obtained when an 1100 UTC initial time was used, and more improvement still when the December/January data were used. Some of the scores were very impressive, reaching above 40% when compared to persistence.

<i>Flight Categories</i>		PERSISTENCE CLIMATOLOGY				PERSISTENCE			
		<i>12Z All</i>	<i>12Z Cool</i>	<i>11Z Cool</i>	<i>11Z Dec/Jan</i>	<i>12Z All</i>	<i>12Z Cool</i>	<i>11Z Cool</i>	<i>11Z Dec/Jan</i>
<i>Ceiling</i>	LIFR	-9.85	2.06	2.82	3.25	24.51	14.89	20.36	23.17
	IFR	-382.57	-13.07	-6.34	-0.21	-199.48	16.84	23.58	17.48
	MVFR	-10.45	-6.24	-0.71	0.54	18.68	21.42	30.01	31.57
	VFR	-27.35	-0.76	2.97	0.91	1.29	16.17	23.00	19.98
<i>Visibility</i>	LIFR	-61.22	21.37	3.42	26.24	4.26	37.13	28.83	47.99
	IFR	-75.76	5.15	-0.58	7.38	-4.71	34.89	28.01	47.22
	MVFR	-36.04	2.47	6.33	2.57	27.13	46.21	49.86	45.48
	VFR	14.06	11.33	8.24	11.01	41.96	32.58	26.81	32.93

Comparisons, such as the skill score, can be helpful when determining relative skill. However, if the benchmark forecast is unreliable, a relative improvement does not necessarily indicate reliable performance in the forecast being tested. It is important, therefore, to look at the actual performance of each individual forecast. In this case, the Brier score is used to check individual performance. Since an observation of an event is either ‘Yes’ (1) or ‘No’ (0), the observation/forecast pairs were divided into a ‘Yes’ observation group and a ‘No’ observation group. The Brier score for each group and each equation set was calculated.

Some basic concepts of the Brier score follow. When using the Brier score with probability forecasts and categorical observations, a perfect forecast will be denoted by $B = 0$, and a perfectly incorrect forecast is denoted by $B = 1$. Since the Brier score is a squared difference, $B \geq 0.25$ indicates an actual difference of ± 0.5 . This implies a 50% or less probability forecast for a ‘Yes’ observation and a 50% or greater forecast for a ‘No’ observation. If we make the broad assumption that 50% is the threshold value for a good forecast in either group, then all forecasts with $B \geq 0.25$ can be considered inaccurate.

Table 2 contains the Brier scores for the second equation set, the 1200 – 1300 UTC forecasts using the cool season data. The values calculated for this set are representative of the values for the other sets. All Brier scores greater than 0.25 in the table are shaded in gray. The most striking feature of the table is that a majority of the Brier

scores in the ‘Yes’ group are above 0.25 and a majority of the scores in the ‘No’ group are below 0.25. The exceptions in both groups are the Brier scores for the VFR forecasts. Performance appears to be positively correlated to the number of observations in the developmental data set (see the table caption for the description).

Table 2. Brier scores for the MLB 12 - 13Z cool season obs-based, persistence climatology, and persistence forecasts using the independent data set. The cool season is defined by the months October through March. The top three rows contain the Brier scores for a 13Z ‘No’ observation, and the bottom three rows contain the Brier scores for a 13Z ‘Yes’ observation. The row above the scores contains the number of observations of each flight category. The dependent data set (dep) contains 3553 observations and the independent (ind) data set contains 911 observations. Gray-filled cells highlight values ≥ 0.25 .

	<i>CLIFR</i>	<i>CIFR</i>	<i>CMVFR</i>	<i>CVFR</i>	<i>VLIFR</i>	<i>VIFR</i>	<i>VMVFR</i>	<i>VVFR</i>
NO (dep)	3253	3315	3162	599	3272	3202	3087	771
(ind)	809	827	778	145	803	796	790	164
Obs	0.0095	0.0057	0.0137	0.3286	0.0064	0.0140	0.0196	0.2235
P-Climo	0.0064	0.0038	0.0117	0.3677	0.0059	0.0070	0.0112	0.2749
Pers	0.0153	0.0163	0.0451	0.3333	0.0244	0.0443	0.0720	0.1731
YES (dep)	190	128	281	2844	172	242	357	2673
(ind)	44	26	75	708	48	55	61	687
Obs	0.3448	0.6182	0.5655	0.0309	0.3336	0.5038	0.6010	0.0362
P-Climo	0.4505	0.7036	0.5943	0.0291	0.4143	0.6381	0.7559	0.0361
Pers	0.3659	0.6154	0.4930	0.0568	0.2093	0.4545	0.6897	0.0916

Table 3. Squared difference medians for the MLB 12 - 13Z cool season obs-based, persistence climatology, and persistence forecasts using the independent data set. The cool season is defined by the months October through March. The top three rows contain the median values for a 13Z ‘No’ observation, and the bottom three rows contain the median values for a 13Z ‘Yes’ observation. The row above the scores contains the number of observations of each flight category. The dependent data set (dep) contains 3553 observations and the independent (ind) data set contains 911 observations. Values ≥ 0.25 are shaded in gray.

	<i>CLIFR</i>	<i>CIFR</i>	<i>CMVFR</i>	<i>CVFR</i>	<i>VLIFR</i>	<i>VIFR</i>	<i>VMVFR</i>	<i>VVFR</i>
NO (dep)	3253	3315	3162	599	3272	3202	3087	771
(ind)	809	827	778	145	803	796	790	164
Obs	0.00007	0.00013	0.00047	0.1686	0.00004	0	0.0015	0.0651
P-Climo	0.0010	0.0005	0.0013	0.1171	0.0001	0.0009	0.0020	0.1400
YES (dep)	190	128	281	2844	172	242	357	2673
(ind)	44	26	75	708	48	55	61	687
Obs	0.1507	0.7347	0.4752	0.0050	0.1467	0.3784	0.5245	0.0020
P-Climo	0.1783	0.9508	0.2732	0.0044	0.2686	0.4018	0.8969	0.0016

Note: Persistence medians were not included. Persistence forecasts are either 0 or 1, therefore the squared difference between an observation and forecast is either 0 or 1. This resulted in a median value of 0 or 1 that was difficult to interpret without graphing the actual distribution.

The Brier score is an average and, like all averages, can be contaminated by outliers in the data. A more robust test of forecast performance may be found in the median of the squared differences, where the median value represents the value at which half of the data points are lower and half of the data points are higher. Table 3 shows the squared difference median values for each of the groups for the same equation set shown in Table 2. Values greater than 0.25 are shaded in gray. The results are similar to the Brier scores in that most of the ‘Yes’ values are above 0.25. The VFR values in the ‘No’ group were not above 0.25, but were higher than the others by two orders of magnitude.

Forecast equations should perform well in both event (‘Yes’) and non-event (‘No’) cases if they are to be used operationally. Tables 2 and 3 demonstrate that while forecasts for non-events were generally good, forecasts for events were highly inaccurate. Thus, these forecast equations in their current form should not be transitioned to operations.

Another step in attempting to improve performance was to use a model other than multiple linear regression (MLR). Logistic regression (LR) is known as an appropriate model for use with binary predictands and was used to develop the 1200 - and 1100 – 1300 UTC cool season equations. The Brier and skill scores from the tests of these equations were very similar to those from the MLR equations. Because LR is more computationally complex than MLR, the tests of LR were discontinued.

Wind Tower Network Data

Dr. Riewe performed the statistical forecasting with the wind tower data in two phases. During the first phase, which is now complete, he applied quality control (QC) methods to data from the KSC/CCAS wind tower network to eliminate questionable data values. In the second phase he developed preliminary statistical forecasting methods and applied them to a subset of the data using the S-PLUS[®] statistical package. A brief description of the QC methods is presented in the following section.

Quality Control

The wind tower data files available for analysis provide 11 years (1986-1996) of data for 67 towers, recorded at five-minute intervals. The files contain temperature, dew point temperature, average wind speed and direction, peak wind speed and direction, and atmospheric pressure. However, there are many missing data entries and many time periods with missing data for specific towers. There are little or no peak wind direction entries in the data files. Another concern is the questionable validity of a small fraction of the values, especially prior to 1994. The goal of the QC phase of the task has been to remove as much questionable data as possible without producing any biases in the data that could affect statistical forecasting. The files produced by the QC process will not only be useful for statistical forecasting, but are also available for other applications.

The QC algorithms perform the following checks to remove questionable data from the wind tower files.

- Limit checks for unrealistic values,
- Deviations from the mean for a given tower, month, and time of day,
- Limits on peak/average speed ratio for winds,
- Meteorological And Range Safety Support (MARSS) vertical check for wind data, and
- Temporal check based on MARSS vertical check for wind data.

All questionable data are replaced by predetermined values that indicate the reason the data were flagged. The QC procedures have been applied to all tower data for the months October through March for the period 1986-1996.

Limit checks

All data with unrealistic values are removed from the data file. The ranges for data to be considered valid are given in Table 4.

Table 4. Allowed ranges for tower data entries.							
	<i>Temperature (C)</i>	<i>Dew Point Temperature (C)</i>	AVERAGE WIND		PEAK WIND		<i>Pressure (kPa)</i>
			<i>Speed (m/s)</i>	<i>Direction (degrees)</i>	<i>Speed (m/s)</i>	<i>Direction (degrees)</i>	
Minimum	-10	-18	0	0	0	0	9600
Maximum	40	35	60	360	70	360	10400

Deviations from the mean

In addition to the broad limit checks, the QC procedure performs comparisons specific to each tower, month, and time of day. For all 11 years of data for a given tower, the data for a single month are combined and the mean and standard deviation are calculated for each five-minute interval of the day. Data are marked as questionable if they differ for the mean for the five-minute time interval by more than the number of standard deviations shown in Table 5. Temperature, dew point, and wind speed are QC'd with this procedure, but wind direction is not.

Table 5. Maximum allowed standard deviations from the mean allowed for tower data for a specific five-minute interval.							
	<i>Temperature</i>	<i>Dew Point Temperature</i>	AVERAGE WIND		PEAK WIND		<i>Pressure</i>
			<i>Speed</i>	<i>Direction</i>	<i>Speed</i>	<i>Direction</i>	
Maximum Allowed Deviation	5	5	10	-	10	-	5

Limits on peak/average speed ratio for winds

An examination of the data sets that had been QC'd by the limit and deviation checks revealed that invalid peak wind speed values were still not being flagged. An example of such anomalous peak wind values can be seen in Table 6, which shows the average wind speed data for the 492-ft level of Tower 313 for the month of January for all years in the period 1986-1996. The values plotted are the number of cases in which the ratio of peak-to-average wind speed (y-axis) corresponds to a specific average wind speed (x-axis). A 'cloud' of anomalous data values can be seen in the upper-right quadrant of the table. Other anomalous values are scattered about in the upper portion of the table. From comparison of the anomalous data with other data in the same time period, it was clear that the peak wind rather than wind speed was almost always invalid in these 'cloud' cases.

Table 6. Ratio of peak-to-average wind speed as function of average wind speed. Anomalous values can be seen especially in the upper right quadrant. Data are for Tower 313 in January for 1986-1996 at 492 ft.

3.0	5	2	0	1	0	0	0	1	1	2	1	2	3	7	0	0	1	1	
2.9	0	0	0	0	0	0	0	0	0	1	1	2	3	0	0	0	0	0	
2.8	0	0	3	1	0	1	1	0	0	3	0	0	7	2	5	0	1	2	
2.7	0	2	0	0	1	0	1	0	0	2	1	1	0	4	4	0	1	1	
2.6	5	0	2	1	0	0	0	1	1	0	3	7	10	9	1	15	1	1	
2.5	0	2	0	4	1	1	0	2	3	4	5	11	8	13	3	3	16	1	
2.4	0	0	2	0	0	0	0	1	0	4	16	18	35	8	15	11	11	24	
2.3	19	0	0	1	0	0	1	0	1	2	21	7	18	36	15	28	20	28	
R	2.2	0	14	8	0	1	2	1	0	1	2	3	20	24	18	29	45	32	98
a	2.1	0	0	0	6	1	5	1	2	1	3	3	3	4	15	10	12	13	56
t	2.0	55	32	19	7	0	2	2	1	2	2	6	2	2	0	2	2	0	29
i	1.9	0	0	0	0	0	0	0	3	8	1	1	0	0	0	1	0	6	
o	1.8	0	0	46	24	7	3	2	7	12	7	1	2	1	0	1	0	1	7
	1.7	0	87	0	0	41	19	4	10	8	17	5	6	0	0	3	0	1	18
	1.6	91	0	129	74	0	40	20	24	8	5	18	18	14	4	1	1	1	22
	1.5	0	162	0	197	126	161	55	81	18	51	22	38	26	35	7	13	4	84
	1.4	0	0	245	0	245	0	160	187	77	67	47	59	120	63	69	15	29	188
	1.3	195	0	0	301	0	328	359	347	201	191	325	126	165	223	107	128	164	673
	1.2	0	309	436	0	382	515	569	600	346	420	403	633	660	272	496	518	585	2846
	1.1	0	0	0	579	643	659	764	879	549	601	597	659	545	1097	1165	1246	1305	7440
	1.0	476	927	908	1029	1148	1269	1227	1226	2336	2477	2227	1954	2176	1931	1784	1595	1505	10165
		3	4	5	6	7	8	9	10	11	12	13	14	15	16	17	18	19	20
		Average wind speed (kt)																	

From the examination of a large number of such tables, an empirical algorithm was developed to screen anomalously high peak wind speeds, as given in Table 7.

Table 7. Algorithm for editing anomalous peak wind speeds. Given the average wind speed range in the left column, if the corresponding ratio in the right column is exceeded, the peak wind speed is flagged.

<i>Average Wind Speed (knots)</i>	<i>Maximum Allowed Value of Peak-to-Average Wind Speed Ratio</i>
< 2	No limit
2	10
3 to 8	2.6 + 0.16(average wind speed)
> 8	2.5 for levels below 50 ft 2.0 for levels 50 ft and above

Vertical consistency check for wind data

The manual examination of peak wind speed data, above, showed that invalid data could often be identified by comparison with similar data recorded at the same time, but at different heights. An algorithm for editing data for different heights at a given time already exists and is used in the present MARSS system to QC wind tower data. The algorithm compares the average wind value to the vector difference of winds at levels above and below the value being checked. The vector difference ΔV_i for the i th tower level is computed from the u - and v -components at three adjoining levels using the equations

$$\Delta u_i = \frac{1}{2}(u_{i-1} + u_{i+1}) - u_i,$$

$$\Delta v_i = \frac{1}{2}(v_{i-1} + v_{i+1}) - v_i, \text{ and}$$

$$\Delta V_i = [(\Delta u_i)^2 + (\Delta v_i)^2]^{1/2}.$$

For the peak wind speed s , the corresponding direction is not usually available, so $\Delta V(p)_i$ is calculated from

$$\Delta V(p)_i = |\frac{1}{2}(s_{i-1} + s_{i+1}) - s_i|.$$

If wind data are missing for either level $i-1$ or $i+1$, then the algorithm uses the next lower or higher level, respectively. The wind speed and direction are designated invalid when $\Delta V_i \geq 15$ kt.

Temporal consistency check for wind data

Because the vertical check requires data at heights both above and below the level being analyzed, much of the tower data cannot be evaluated. However, there is no such limitation on temporal data checking. The temporal check uses the same algorithm as the vertical check, but the subscripts $i-1$, i , and $i+1$ correspond to data at three five-minute time intervals centered on the data being evaluated. If values are missing at times $i-1$ or $i+1$, the algorithm uses the next earlier or later value, respectively. As with the vertical check, the wind speed and direction are designated invalid when $\Delta V_i \geq 15$ kt.

References

Vislocky, R.L., and J.M. Fritsch 1997: An automated, observations-based system for short-term prediction of ceiling and visibility. *Wea. Forecasting*, **12**, 31-43.

2.3 TASK 004 INSTRUMENTATION AND MEASUREMENT

SUBTASK 5 I&M AND RSA SUPPORT (DR. MANOBIANCO AND MR. WHEELER)

No work was performed on this task during the quarter.

SUBTASK 10 EVALUATION OF WIND PROFILER DATA (DR. MANOBIANCO)

The AMU began an option hours task, funded by KSC in April 1999, to evaluate the accuracy and reliability of data collected from a 'Hypersodar' for eight days covering the periods 28 October – 2 November 1998 and 16 – 17 March 1999. Dr. Manobianco completed revisions to the final report in September 1999. It will be published as a NASA contractor report in October 1999. Excerpts from the final report are included in the following subsections.

Introduction

The AMU was tasked to collect the best available data for comparison from the Eastern Range wind towers and 915-MHz profilers and perform an evaluation of the accuracy and reliability of the sodar. NASA supplied the following sodar data in textual format.

- Two-minute-averaged sodar data from 16 March 1999 and two 5-minute-averaged data files from 17 March 1999.
- One 5-minute data from 1715:00 – 2055:00 UTC 17 March 1999 and 5-minute sodar data from 2140:00 UTC 17 March – 0420:00 18 March 1999.
- One-second data from 1832:07 – 1902:49 UTC 16 March 1999 computed by Method B.
- One-second data from 1904:56 – 1937:40 UTC 16 March 1999 computed by Method C.
- One-, 5-, and 10-minute data from 28 October 1998 – 2 November 1998.

During the data collection periods, the sensor was located adjacent to tower 412 near the SLF. At this location, the sensor was approximately 4.5 km from the Merritt Island (MI) 915-MHz profiler, 7.8 km from the False Cape (FC) 915-MHz profiler, and 3.5 km from tower 313 (Figure 6). Although the sensor was closest to tower 412, this tower only measures wind speed and direction at 3.7 and 16.5 m. Therefore, sensor data were obtained from tower 313 that provides wind speed and direction measurements up to 150 m. The AMU received all available 5-minute and 1-minute data from towers 412 and 313 for the period of interest from Computer Sciences Raytheon (CSR).

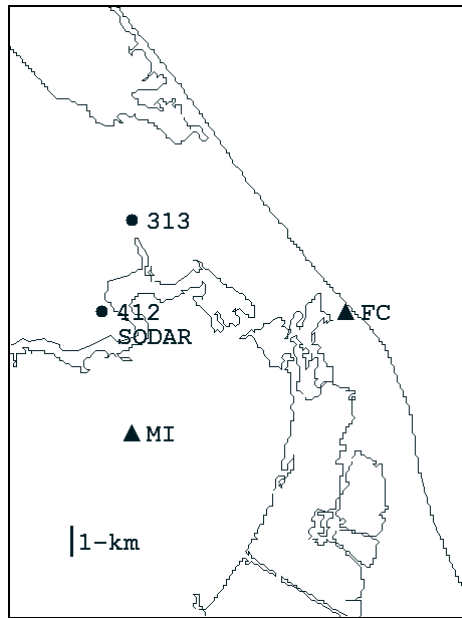


Figure 6. Map showing locations of the sodar (SODAR), towers, 412 and 313, and False Cape (FC) and Merritt Island (MI) 915-MHz profilers.

The sensor was closest to the MI 915-MHz profiler. However, data were available from the MI profiler for only 3 of the 8 days that sensor data were collected (see Table 8). For this reason, data were obtained from the FC profiler for the entire 8-day period (Table 8). The FC profiler is located adjacent to the Atlantic Ocean while the MI profiler is located inland by roughly 8.2 km.

Table 8. Data availability for the periods of interest ('X' indicates data are available from the particular instrument on the given date).				
Date	915-MHz Profilers		KSC /CCAS Towers*	
	Merritt Island	False Cape	412	313
10/28/98	X	X	X	X
10/29/98	X	X	X	X
10/30/98	X	X	X	X
10/31/98		X	X	X
11/1/98		X	X	X
11/2/98		X	X	X
3/16/99		X	X	X
3/17/99		X	X	X

*Includes both 5-minute and 1-minute data

The sodar was initially co-located with tower 412, but its orientation and position were changed during both the 1998 and 1999 sampling periods. For all orientation adjustments, the sodar was not aligned with true north. Consequently, the bias in wind direction computed between the sodar and 915-MHz profiler or tower data contains a systematic component that is constant with height and reflects changes in sodar orientation. Without quantitative information regarding the orientation of the sodar relative to true north, it is not possible to isolate and remove the systematic (alignment) bias from total instrument bias. For the purpose of this evaluation, the bias and RMS difference statistics do not account for changes in sodar location.

Data Quality Control

QC of the sodar data was accomplished based on the signal-to-noise (SNR) ratio and quality (Q) flags provided by the vendor. As specified by NASA in the Statement of Work (SOW), sodar data were not used when the SNR < 2 dB and Q < 0.6 for the u, v, or w wind components. The sodar data files from 28 October 1998 – 2 November 1998 already contained values of 999999 that were assumed to designate points failing the SNR and Q checks as identified by the vendor. The 915-MHz profiler data from the Merritt Island and False Cape sites were quality controlled using algorithms discussed in Lambert and Taylor (1998). Additional QC of the sodar, tower, and 915-MHz profiler observations, including identification and removal of unrealistic values, was accomplished by visual inspection.

Evaluation Protocol

The SOW required the calculation of bias and RMS difference as a function of height for sodar wind speed and direction as well as sodar data availability as a function of height. The bias and RMS differences in wind speed and direction were computed separately using scalar averaging as discussed by Merceret (1995). The differences between sodar and tower or 915-MHz profiler observations at a given level are defined as $\Phi' = \Phi_s - \Phi_o$. Here, the subscripts *s* and *o* denote sodar and tower or 915-MHz profiler quantities, respectively. The bias is computed using N pairs of observations for each data set at a given vertical level as:

$$\overline{\Phi'} = \frac{1}{N} \sum_{i=1}^N \Phi'_i$$

and the RMS difference is computed as:

$$\text{RMSE} = \left[\frac{1}{N} \sum_{i=1}^N (\Phi'_i)^2 \right]^{1/2}$$

Note that the RMS difference includes bias and no attempt is made in this evaluation to compute and display bias-corrected RMS differences.

For the tower comparisons, the available discrete heights are compared to the closest available gates of the sodar. For the 915-MHz profiler comparisons, the sodar data are averaged temporally and spatially to match the gate spacing and time intervals of the profiler data. The averaging procedure is applied before computing the bias and RMS differences. The bias and RMS differences are not computed if the SNR < 2 dB and Q < 0.6 or the missing value flag of 999999 is present in the sodar data files. The data availability as a function of height is computed as a ratio of sodar observations passing the QC checks to the total number of observations possible for each data collection period.

Sodar data are excluded from the spectral analysis when the SNR < 2 dB and Q < 0.6 for the u, v, or w wind components. In order to perform Fourier transforms for the spectral analysis, it is necessary to interpolate for missing data or data removed by the QC checks. The interpolation in time is performed using a cubic spline. Spectral response is calculated by first removing the mean from the interpolated sodar data. The wind speed data are then divided into roughly five-minute periods, Fourier transformed, and averaged to produce the spectral density which is plotted against frequency. The spectral graphs and related discussion are not included here but can be found in the final report.

Results

The proposed level of effort for the evaluation did not include time required to address unexpected issues with sodar data formats. For example, the time convention was local rather than UTC, there were eight separate reporting periods, and there were three different file formats. These issues complicated the collection, processing, and QC of sodar data. Consequently, the AMU underestimated the amount of time required to complete this task. Due to these time constraints, the AMU completed only the following tasks.

- Computation of bias and RMS differences for the two sets of 5-minute sodar data from 17 – 18 March 1999.
- Computation of bias and RMS differences for 5-minute sodar data from 2 – 3 November 1998.
- Spectral analysis of the 1-second Method B and Method C sodar data from 16 March 1999.

Although the sodar was located adjacent to tower 412, comparisons between tower 412 and the sodar were not useful because the lowest sodar gate is above the highest sensor on tower 412. Additionally, comparisons between the sodar and False Cape 915-MHz profiler using sodar data collected on 17 March 1999 resulted in bias and RMS differences which were generally much larger than those computed from sodar and tower 313 data. This result was not surprising because the sodar and False Cape 915-MHz profiler were separated by a distance of about 7.8 km (Figure 6). Furthermore, only the lower 915-MHz profiler and upper sodar gates were used to compute the bias and RMS differences. The sodar data at these levels were least reliable and often flagged by QC checks. Given these limitations and results from preliminary comparisons, additional calculations of bias and RMS differences were not performed using either the False Cape or Merritt Island 915-MHz profiler observations.

Summary of Bias and RMS Difference Statistics

The bias, RMS differences, and standard deviations in wind speed and direction from sodar wind solution B and tower 313 northeast (NE) sensor are summarized in Table 9. Sodar wind solution B is chosen because it does not contain the erroneous estimates of wind speed and direction identified during the 17 - 18 March 1999 data collection period (see sections 2.2.3 and 2.2.4 of the final report). The bias, RMS differences, and standard deviations computed from the sodar and tower observations at White Sands Missile Range (WSMR) are included in Table 10. These data were collected by the vendor during selected periods from 22 – 30 September 1998. It is important to note that the sodar was aligned with north during that time and separated from the WSMR tower by a distance of 450 m. The statistics from WSMR are included here for comparison with those derived from sodar and tower 313 observations. There are three essential points that must be considered in comparing statistics shown in Tables 9 and 10.

- The bias, RMS differences, and standard deviations from the KSC data set are based on 5-minute averaged sodar data while those from WSMR are based on 10-minute averaged data.
- The wind direction statistics from the KSC data sets contain a systematic bias because no attempt was made to align the instrument with true north.
- At KSC, the sodar was located ~3.5 km from tower 313 whereas at WSMR, it was located 450 m from the tower. In addition, the potential for noise to contaminate the sodar wind estimates is greater at KSC than at WSMR.

Table 9. Summary of bias, RMS differences, and standard deviations from sodar and tower 313 NE sensor comparisons for periods listed below. Summary statistics from 17 – 18 March 1999 are from only sodar wind solution B. Standard deviations are computed as $(\text{RMS}^2 - \text{Bias}^2)^{1/2}$.

5-Minute Sodar Data (1715:00 – 2055:00 UTC 17 March 1999)							
Height (m)	Wind Speed			Wind Direction			Number of Samples
	Bias (m s^{-1})	RMS Difference (m s^{-1})	Standard Deviation (m s^{-1})	Bias (degrees)	RMS Difference (degrees)	Standard Deviation (degrees)	
50	-0.37	0.78	0.69	-17.0	19.5	9.6	45
65	-0.52	0.83	0.65	-17.9	20.3	9.6	45
95	-0.05	0.80	0.80	-16.7	19.2	9.5	45
125	0.04	0.65	0.65	-13.3	16.8	10.3	43
155	0.36	0.79	0.70	-11.3	13.9	8.1	39
5-Minute Sodar Data (2140:00 UTC 17 March – 0420:00 UTC 18 March 1999)							
Height (m)	Wind Speed			Wind Direction			Number of Samples
	Bias (m s^{-1})	RMS Difference (m s^{-1})	Standard Deviation (m s^{-1})	Bias (degrees)	RMS Difference (degrees)	Standard Deviation (degrees)	
50	-0.68	0.90	0.59	-27.8	29.0	8.3	81
65	-1.10	1.48	0.99	-30.8	32.3	9.7	81
95	-1.37	1.83	1.21	-24.8	28.1	13.2	78
125	-1.25	1.70	1.15	-13.8	25.4	21.3	63
155	-0.91	1.33	0.97	-6.2	25.4	24.6	51
5-Minute Sodar Data (2250:00 UTC 2 November – 0405:00 UTC 3 November 1998)							
Height (m)	Wind Speed			Wind Direction			Number of Samples
	Bias (m s^{-1})	RMS Difference (m s^{-1})	Standard Deviation (m s^{-1})	Bias (degrees)	RMS Difference (degrees)	Standard Deviation (degrees)	
50	-0.77	1.07	0.74	-2.7	4.5	3.6	64
75	-0.70	0.98	0.69	-1.5	4.5	4.2	64
100	-1.29	1.57	0.89	-2.6	4.8	4.0	64
125	-1.79	2.04	0.98	-4.2	6.8	5.4	64
150	-1.76	1.97	0.89	-0.9	6.8	6.7	62

Table 10. Summary of bias, RMS differences, and standard deviations from the sodar and tower measurements at White Sands Missile Range. Standard deviations are computed as $(\text{RMS}^2 - \text{Bias}^2)^{1/2}$. These statistics are used with permission from Dr. P. Chintawongvanich (Sensor Technology Research, Inc.) and adapted from his NASA SBIR Phase II final report briefing given on 21 April 1999.

10-Minute Sodar Data (22 – 30 September 1998)								
Wind Speed					Wind Direction			
Height (m)	Bias (m s^{-1})	RMS Difference (m s^{-1})	Standard Deviation (m s^{-1})	Number of Samples	Bias (degrees)	RMS Difference (degrees)	Standard Deviation (degrees)	Number of Samples
50	0.19	0.61	0.58	219	-2.1	10.5	10.3	209
75	-0.12	0.49	0.48	226	-3.1	10.2	9.7	211
100	-0.34	0.62	0.51	224	-1.0	10.9	10.8	214
125	-0.38	0.69	0.58	223	2.9	11.4	10.9	212
150	0.34	0.64	0.54	216	-2.5	12.0	11.7	213

Table 11. Summary of bias and RMS differences from tower 412 and tower 313 NE at 16.5 m for periods listed below. Standard deviations are computed as $(\text{RMS}^2 - \text{Bias}^2)^{1/2}$.

5-Minute Tower Data (1715:00 – 2055:00 UTC 17 March 1999)							
Wind Speed				Wind Direction			Number of Samples
Height (m)	Bias (m s^{-1})	RMS Difference (m s^{-1})	Standard Deviation (m s^{-1})	Bias (degrees)	RMS Difference (degrees)	Standard Deviation (degrees)	
16.5	-0.21	0.66	0.63	-17.9	21.9	12.6	45
5-Minute Tower Data (2140:00 UTC 17 March – 0420:00 UTC 18 March 1999)							
Wind Speed				Wind Direction			Number of Samples
Height (m)	Bias (m s^{-1})	RMS Difference (m s^{-1})	Standard Deviation (m s^{-1})	Bias (degrees)	RMS Difference (degrees)	Standard Deviation (degrees)	
16.5	-0.68	0.90	0.59	-2.5	7.8	7.4	51
5-Minute Tower Data (2250:00 UTC 2 November – 0405:00 UTC 3 November 1998)							
Wind Speed				Wind Direction			Number of Samples
Height (m)	Bias (m s^{-1})	RMS Difference (m s^{-1})	Standard Deviation (m s^{-1})	Bias (degrees)	RMS Difference (degrees)	Standard Deviation (degrees)	
16.5	0.20	0.54	0.50	-3.9	5.3	3.6	62

The wind speed and direction biases at WSMR and KSC include a contribution due to the distance between the sodar and towers. The biases due to sensor separation at KSC are estimated by computing differences in wind measurements between tower 412 adjacent to the sodar and tower 313 at 16.5 m (Table 11). In comparing the WSMR and KSC statistics shown in Tables 9 – 11, it is assumed that wind variability generally decreases with height. Therefore, tower 412 and 313 comparisons at 16.5 m represent an upper bound on the magnitude of wind speed and direction differences due to spatial separation. Furthermore, biases at WSMR are assumed to result primarily from instrument error and not spatial separation, thereby providing an upper limit on instrument error. It is not possible to quantify further the magnitude and vertical profile of biases due to sensor separation from the data available at either KSC or WSMR.

If the estimated speed biases due to spatial separation (Table 11) are used to modify the values shown in Table 10, the resulting speed biases at KSC range from about $-2 - 0.6 \text{ m s}^{-1}$. In comparison, the speed biases at WSMR range from $-0.38 - 0.34 \text{ m s}^{-1}$ (Table 10). During the three data collection periods examined for this evaluation, the KSC sensor separation-adjusted speed biases at certain times and levels are comparable to those from WSMR. However, at other times and levels, the adjusted speed biases at KSC exceed those at WSMR by more than 1.0 m s^{-1} suggesting that results at KSC are not entirely consistent with those from WSMR. A similar conclusion is apparent when analyzing the wind direction biases at KSC and WSMR given that there is also an alignment bias at KSC.

It is interesting to note that during 2 – 3 November 1998, the wind speed bias and RMS differences are largest while the wind direction bias and RMS differences are smallest in comparison with other statistics shown in Table 9. Although sodar alignment can explain a portion of these differences, wind regime is also a likely cause. Average wind speeds from 2 – 3 November are larger compared with all other collection periods at KSC (not shown). Under these conditions, wind direction variability is likely to be smaller than during weaker wind regimes. On the other hand, wind speed variability would be greater due to frictional effects and distance from the coast. For the 2 - 3 November 1998 data collection period, the average wind direction of $\sim 135 - 140^\circ$ has a significant onshore component (not shown). Therefore, average wind speeds would tend to be greater at tower 313 closer to the coast than further inland at the sodar site. In fact, the average wind speed plots for 2 – 3 November (not shown) support this statement and suggest that spatial separation between the sodar and tower 313 could account for the larger wind speed bias and RMS differences.

Summary and Conclusions

The previous sections highlight the AMU evaluation of a sodar wind profiler located on KSC adjacent to tower 412. The sodar data used for this evaluation were collected during two different periods in March 1999 and November 1998. The sodar orientation and position were changed twice during the data sampling periods considered in this study. In neither case was any attempt made to align quantitatively the sodar with true north. Therefore, it is not possible to account for (and remove) any systematic alignment bias from total instrument bias.

The evaluation is performed by calculating sodar data availability as a function of height and bias and RMS differences versus height using 5-minute averaged sodar data and observations from tower 313. The bias and RMS differences are compared with those obtained by the vendor using 10-minute averaged sodar and tower data collected at WSMR. Finally, a spectral analysis of 1-second sodar data is performed to highlight the true temporal resolution of the data by differentiating between the noise and wind signals in the observations.

Direct comparisons of sodar and tower 412 data are not useful because the lowest sodar gate at 50 m is above the highest sensor at 16.5 m on tower 412. Therefore, tower 313 is used for the bias and RMS difference computations because it provides wind speed and direction measurements up to 150 m. As shown in Figure 6, tower 313 is located ~ 3.5 km to the north-northeast of the sodar site. Comparisons of sodar and 915-MHz boundary layer wind profiler data are also not shown for the following reasons.

- The closest profiler is more than 4 km from the sodar.
- Only the highest gates of the sodar overlap with the lowest two gates of the 915-MHz profilers.

- Data are often flagged by QC checks and are least reliable at the highest sodar gates.

The following conclusions can be drawn from the evaluation.

- Using the SNR and Q checks or missing value flags, sodar data availability (not shown) is generally near 100% below 100 m but decreases rapidly above 100 m and is typically less than 50% above 200 m. Signal processing and QC methods not solely dependent on the SNR may improve the data availability statistics as well as ensure data which pass the vendor QC checks are not contaminated.
- The wind speed biases between tower 313 and wind solution B vary by height and time period and range from $-1.79 - 0.36 \text{ m s}^{-1}$. The standard deviations in wind speed for solution B at all time periods and heights range from $0.59 - 1.15 \text{ m s}^{-1}$. The RMS differences in wind speed for solution B at all time periods and heights range from $0.65 - 2.04 \text{ m s}^{-1}$. Note that RMS differences are not bias-corrected.
- The wind direction biases between tower 313 and sodar solution B for all time periods and heights are negative and range from $-30.8 - -0.9^\circ$. The standard deviations in wind direction for solution B at all time periods and heights range from $3.6^\circ - 24.6^\circ$. The RMS differences in wind direction range from $4.5 - 32.3^\circ$. Note that RMS differences are not bias-corrected.
- For the second 5-minute sodar data set collected during 17 – 18 March 1998 (not shown), solution A produces wind estimates that are inconsistent with those from solution B or tower 313 observations. The SNR and Q checks did not flag these winds therefore some other form of quality control is needed to identify erroneous data that may have acceptable SNR.
- Overall, the differences between tower 313 and sodar wind observations for the limited samples examined in this evaluation are due to misalignment of the sodar, variability in wind over the 3.5-km distance separating the two instruments, and instrument error. It is not possible to identify accurately the systematic errors due to alignment and spatial separation given the available data collected at KSC.
- Spectral response at all levels (not shown) suggests that the sodar is able to resolve features down to the Nyquist frequency which is 0.5 Hz (2-second period) for the data sets examined in this evaluation.

The RMS differences in wind speed and wind direction from sodar wind solution B at KSC range from $0.65 \text{ m s}^{-1} - 2.04 \text{ m s}^{-1}$ and $4.5 - 32.3^\circ$, respectively. Note that these RMS differences are not bias-corrected. The vendor claims that the accuracy of the wind measurements from the sodar is better than 0.5 m s^{-1} in speed and 10° in direction (Sensor Technology Research, Inc. NASA SBIR phase II final report briefing). The results of the evaluation described here suggest that such accuracy may be attainable though the data available for this comparison made it impossible to confirm the vendor's claims. The sodar was not aligned with true north and was separated by a distance of 3.5 km from tower 313 used for comparisons in this study.

During the three data collection periods examined for this evaluation, the KSC sensor separation-adjusted wind speed and direction biases at certain times and levels are comparable to those from WSMR. However, at other times and levels, the adjusted speed biases at KSC exceed those at WSMR by more than 1.0 m s^{-1} . These statistics suggest that results at KSC are not entirely consistent with those from WSMR given the differences in spatial separation between the sodar and tower at each site.

References

Lambert, W. L., and G. E. Taylor, 1998: Data quality assessment methods for the Eastern Range 915-MHz profiler network. NASA Contractor Rep. CR-1998-207906, 49 pp.

Merceret, Francis J., 1995: The effect of sensor sheltering and averaging techniques on wind measurements at the Shuttle Landing Facility. NASA TM-111262, 42 pp.

2.4 TASK 005 MESOSCALE MODELING

SUBTASK 4 DELTA EXPLOSION ANALYSIS (MR. EVANS)

The Delta Explosion Analysis project is being funded by KSC under AMU option hours. Mr. Evans is completing revisions of the draft final report on the Delta II explosion. The draft will go to the 45th Weather Squadron (45 WS) and the 45th Space Wing (45 SW) for review in October.

SUBTASK 8 MESO-MODEL EVALUATION (MR. CASE)

During the past quarter, the Regional Atmospheric Modeling System (RAMS) component of the Eastern Range Dispersion Assessment System (ERDAS) was run in real-time and evaluated for the months of April–August. Mr. Dianic gathered forecast data from 0000 UTC and 1200 UTC initialization runs as part of the objective component of the ERDAS RAMS evaluation. He computed average quantities, bias, mean absolute and root mean square errors, and standard deviations for the u- and v-wind components, wind speed and direction, temperature, and dew point temperature. These quantities were computed at the KSC/CCAS wind tower network and standard surface stations across the southeastern United States.

Mr. Wheeler performed the subjective component of the ERDAS RAMS evaluation to verify RAMS forecasts of the central Florida east coast sea breeze (ECSB), precipitation, and low-level temperature inversions. Forecaster and Launch Weather Officer (LWO) participation was encouraged during Mr. Wheeler's daily subjective evaluations. On several occasions, the duty forecaster, LWO, or radar operator inquired about the model guidance in precipitation forecasts on the 1.25-km grid.

The ERDAS RAMS model could not be run locally during most of September for two reasons. First, Alden Electronics Inc. announced in late August that they would no longer transmit gridded data via satellite beginning 1 November 1999. In response, CSR reconfigured the Meteorological Interactive Data Display System for UNIX (MIDDS-X) to ingest and decode gridded data from the NOAAPORT Broadcast System (NBS) rather than Alden Electronics Inc. The format of the gridded Eta data from NBS is different than the format from Alden Electronics Inc. Therefore, modifications to the Eta gridded data were necessary in order to use these data as boundary conditions for ERDAS RAMS. Second, Year 2000 (Y2K) tests were performed on MIDDS-X over the course of several days. All of the modifications and tests for MIDDS-X were not completed until late September and as a result, the ERDAS RAMS sea breeze and precipitation verification statistics were not collected for September.

Mr. Dianic and Mr. Wheeler provided Mr. Case with all the data compiled for the warm-season months of May–August. Mr. Case prepared all the objective and subjective evaluation data at 13 selected KSC/CCAS towers and wrote a preprint article that will be presented at the American Meteorological Society 80th Annual Meeting in January 2000. The article is entitled Evaluation of RAMS in the Eastern Range Dispersion Assessment System, and will be published in the preprint volume of the 11th Joint Conference on the Applications of Air Pollution Meteorology with the Air and Waste Management Association. The paper focuses on the objective evaluation of forecast winds and temperature and the subjective evaluation of the forecast ECSB onset and propagation at the 13 selected KSC/CCAS towers during the months of May–August. A modified version of the preprint article appears below.

Introduction

The following sections describe the AMU's preliminary evaluation of the RAMS component of ERDAS. RAMS is described in more detail by Pielke et al. (1992) and ERDAS by Lyons and Tremback (1994). ERDAS is designed to provide emergency response guidance for operations at KSC/CCAS in the event of a hazardous material release or an aborted vehicle launch. The prognostic gridded data from RAMS is available to ERDAS for display and input to the Hybrid Particle and Concentration Transport (HYPACT) model. The HYPACT model provides three-dimensional dispersion predictions using RAMS forecast grids. Therefore, the accuracy of the HYPACT model is highly dependent upon the accuracy of RAMS forecasts.

The primary goal of the evaluation is to determine the accuracy of RAMS forecasts during all seasons and under various weather regimes. The evaluation protocol is based on the needs of Eastern Range safety and weather personnel and is designed to provide specific information about the capabilities, limitations, and daily use of ERDAS RAMS for operations at KSC/CCAS. The ERDAS RAMS evaluation primarily concentrates on wind and temperature (stability) forecasts which are required for dispersion predictions using the HYPACT model. When the evaluation is completed in the beginning of 2001, operational users will have on-line tools and information in the form of evaluation results to help interpret and apply forecast data from ERDAS RAMS. The results presented here include a portion of the evaluation focusing on the verification of winds and the timing of sea-breeze passage over east-central Florida.

Model description and configuration

RAMS is a dynamical numerical weather prediction model with optional parameterization schemes for representing physical processes in the atmosphere. The model may be run in two or three dimensions and in hydrostatic or non-hydrostatic modes. RAMS features a terrain-following vertical coordinate, a variety of lateral and upper boundary condition options, and capabilities for mixed-phase microphysics.

In the ERDAS configuration, the three-dimensional, non-hydrostatic mode of RAMS is run on four grids with resolutions of 60, 15, 5, and 1.25 km (Figure 7). The lateral boundary conditions are nudged (Davies 1983) by 12–36-h forecasts from Eta model data on an 80-km grid. Two-way interaction is utilized on the inner three nested grids. The physical parameterization schemes used in ERDAS RAMS include a microphysics scheme following Cotton et al. (1982), a modified Kuo cumulus convection scheme (Tremback 1990), Chen and Cotton (1988) radiation, Mellor and Yamada (1982) type turbulence closure, and an 11-layer soil-vegetation model (Tremback and Kessler 1985) with fixed soil moisture in the initial condition. The modified Kuo scheme is run on grids 1-3 and microphysics is run on all four grids.



Figure 7. The real-time ERDAS RAMS domains are shown for (a) the 60-km mesh grid (Grid 1) covering much of the southeastern United States and adjacent coastal waters, (b) the 15-km mesh grid (Grid 2) covering the Florida peninsula and adjacent coastal waters, (c) the 5-km mesh grid (Grid 3) covering east-central Florida and adjacent coastal waters, and (d) the 1.25-km mesh grid (Grid 4) covering the area immediately surrounding KSC/CCAS.

ERDAS RAMS is initialized twice-daily at 0000 UTC and 1200 UTC using Eta 12-h forecast grids and operationally-available observational data including rawinsondes, surface stations and buoys, and KSC/CCAS towers, 915-MHz profilers, and the 50-MHz profiler. No variational data assimilation scheme or nudging technique is applied when incorporating observational data; each forecast is initialized with a ‘cold start’. ERDAS RAMS is run in real-time for a 24-h forecast period on three Hewlett Packard (HP)-K460 workstations with a total of 11 parallel processors. The operational cycle requires approximately 15 minutes of wall-clock time to analyze observational data for the initial condition and 10-12 h to complete the 24-h forecast cycle. On many occasions

when the model produced extensive convection, a 24-h forecast took longer than 12 h to complete due to intensive calculations associated with the microphysics scheme. In these instances, the existing ERDAS RAMS run is terminated and the new simulation begins. Consequently, ERDAS RAMS data are occasionally missing from the 22–24-h forecasts. In the event of a 1-cycle failure, prognostic data are still available from the previous forecast cycle.

Methodology

The AMU evaluation of ERDAS RAMS during the 1999 warm season includes an objective and subjective component. The objective component compares analysis and forecast gridded data of wind at 16.5 m (54 ft) only over the area of grid 4 covered by the KSC/CCAS wind tower network. Also, 0–24-h forecasts of wind, temperature, and moisture are compared with surface land, buoy, KSC/CCAS tower, rawinsonde, and 915 MHz and the 50 MHz profiler data at all available observation locations on grid 4, and selected surface and rawinsonde stations on grids 1-3. Furthermore, sensitivity tests are conducted to assess the influence of initial conditions and physical parameterization schemes on the quality of ERDAS RAMS forecasts. The objective results presented in this quarterly report only include point statistics of grid 4 forecasts of winds and temperatures at 13 selected KSC/CCAS towers (Figure 8).

An automated tool was developed to save forecast grids from twice-daily ERDAS RAMS simulations and to compute and archive real-time error statistics of model forecasts. Wind forecasts from grid 4 were interpolated to 16.5 m (54 ft) and point error statistics were computed at the 13 selected KSC/CCAS tower observations given in Figure 8. Temperature forecasts from grid 4 were interpolated to 1.8 m (6 ft) and corresponding point error statistics were computed for the 13 selected KSC/CCAS tower sites. In addition, the averages of forecasts and observations of selected meteorological variables were computed as a function of forecast hour over all 13 KSC/CCAS towers for the entire four-month evaluation period.

The point statistics presented in this quarterly include the averages of forecasts and observations, bias (forecast – observed), error standard deviation (SD), and RMS error for u- and v-wind components, wind direction, and temperature. Special care was exercised when computing the mean and SD of wind-direction errors following Turner (1986). Error statistics for all other variables were calculated in a traditional manner.

The subjective evaluation verifies ERDAS RAMS forecasts of the onset and movement of the central Florida east coast sea breeze (ECSB), precipitation, and low-level temperature on grid 4. Valid ERDAS RAMS forecasts for the subjective verification include 0000 UTC and 1200 UTC forecasts on grid 4 from all four warm-season months, but only for normal working days and successful model runs. Only the verification of the forecast ECSB for the 1999 Florida warm season (May–August) is discussed here.

The timing of the forecast ECSB is verified to the nearest hour at the 13 selected KSC/CCAS observational towers shown in Figure 8. Both GOES-8 satellite imagery and Weather Surveillance Radar-1988 Doppler (WSR-88D) data were used to identify the occurrence of the ECSB. To check for a sea-breeze passage, coastal KSC/CCAS towers were examined for a shift to an onshore wind (wind direction between 330° and 150°). KSC/CCAS towers further inland were checked for the development and maintenance of a wind shift from a westerly to an easterly component. During easterly flow regimes, sea-breeze passages were classified as an increase in the negative (easterly) u-wind component at each KSC/CCAS tower. The same wind criteria for identifying the observed ECSB passage were applied to the ERDAS RAMS forecasts interpolated to each KSC/CCAS tower location.

A contingency table was developed based on only the observed and forecast occurrence of the central Florida ECSB at any of the 13 KSC/CCAS towers. A ‘hit’ was assigned when an observed and forecast sea breeze passage occurred at any KSC/CCAS tower. Given a sea breeze within the KSC/CCAS network, the onset and movement of the sea breeze was verified to the nearest hour at each of the 13 KSC/CCAS towers. Statistics were generated for the sea-breeze timing verification including RMS errors, error SD, and bias. Categorical and skill scores as defined in Schaefer (1990) and Doswell et al. (1990), and error statistics for the subjective verification of the forecast ECSB timing are presented in the subjective verification of the sea breeze section.

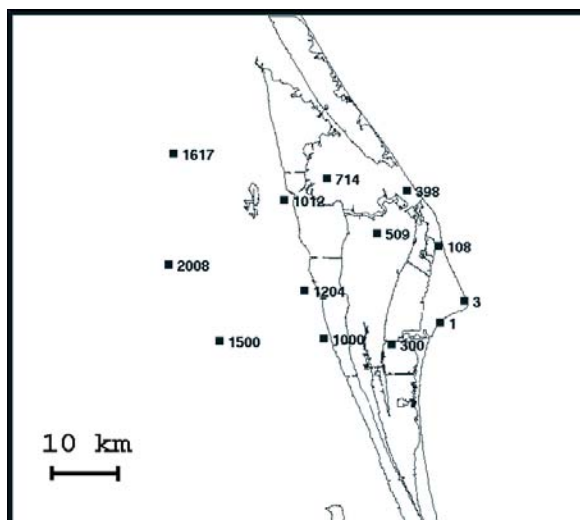


Figure 8. The locations of the 13 KSC/CCAS wind towers used for the objective and subjective verification statistics are shown along with the respective tower identification numbers.

Objective verification statistics

In this section, average quantities and point error statistics are presented for the 1999 warm-season months (May–August). Because the error statistics exhibited similar behavior during each month, cumulative results are shown for the entire period rather than for each individual month. For purposes of interpretation, total model error (RMS error) includes contributions from both systematic and non-systematic errors. Systematic error (bias) can be caused by a consistent misrepresentation of physical parameters such as radiation and convection. Nonsystematic errors are given by the error SD and represent the random errors caused by uncertainties in the model initial condition or unresolvable differences in scales between the forecasts and observations.

In the four months of the objective evaluation, the maximum possible number of verification points for each forecast hour is 1599 (13 towers \times 123 days). However, the actual number of points in the verification data set is between 1007 and 1228 for each forecast hour from 0–21 h. The reduction in verification points resulted from system failures and deficient or missing Eta forecasts which are required to initialize ERDAS RAMS. The number of data points decrease even further during forecast hours 22, 23, and 24 (between 500 and 600 data points by 24 h) because many model runs did not finish in 12 hours before the subsequent model run began.

The average forecast u- and v-wind components exhibit a close correspondence to the observed trends throughout the 24-h ERDAS RAMS forecast period (Figure 9a1). The forecast u-wind experiences an easterly (negative) bias as large as 2 m s^{-1} , primarily after the 15-h forecast (Figure 9a2). The v-wind component exhibits a slight southerly (positive) bias, again primarily after the 15-h forecast (Figure 9a2). The SD and RMS errors of the u- and v-winds increase noticeably after the 15-h forecast (Figure 9a3-4). Furthermore, forecast wind speeds after 15-h exhibit a positive bias between 1.0 and 1.5 m s^{-1} (not shown). The central Florida ECSB typically propagates westward through the KSC/CCAS tower network during the late morning and early afternoon hours (1500–1800 UTC, Cetola 1997) corresponding to the 15–18-h forecasts from the 0000 UTC ERDAS RAMS run. Therefore, these results suggest that the forecast wind speeds are slightly too strong following the passage of the central Florida ECSB. This statement is supported by the easterly u-wind bias shown in Figure 9a2.

The graphs in Figure 9a show that the magnitudes of the RMS errors are typically on the order of the magnitudes of the average u- and v-wind components. In some instances, these errors could result in a sign change between individual forecast and observed wind components, especially during light wind regimes. These results may have implications on the utility of RAMS in operational forecasts and toxic dispersion modeling.

The RMS error for wind direction from the 0-h ERDAS RAMS forecast is about 25° (Figure 9b4) whereas the bias at this time is less than 5° (Figure 9b2). In addition, the 0-h SD in wind direction is nearly the same magnitude

as the RMS error (Figure 9b3-4) suggesting that the total error is due to non-systematic variability in the forecasts and/or observations. A previous study at the NASA Shuttle Landing Facility showed that the SD in wind direction from the KSC/CCAS towers is inversely proportional to the square root of wind speed (Merceret 1995). Based on this formulation, the SD in observed wind direction is estimated to be 15–23° using the average observed tower wind speeds (not shown). Therefore, much of the 0-h RMS error in wind direction from ERDAS RAMS is likely due to the expected variance in the tower observations.

With the exception of the nocturnal and early morning hours when wind speeds are light (6–15-h forecast), the average observed and forecast wind direction trends are in close agreement (Figure 9b1). The bias is on the order of $\pm 5^\circ$, which is negligible compared to the magnitude of the RMS error. In addition, the SD is very close to the magnitude of the RMS error which approaches 50–70° after 3-h (Figure 9b3-4). Thus, non-systematic random errors comprise most of the total error in forecast wind direction. It is important to note that approximately 15–23° of the 50–70° RMS errors in wind direction are likely due to variability in the tower observations. After accounting for variance in observations, the remaining RMS errors in wind direction are on the order of 35–55°. These errors may result from the model's inability to resolve explicitly the small-scale turbulent eddies, especially those associated with light and variable wind regimes during the nocturnal and early morning hours.

The wind direction errors for the 0000 UTC ERDAS RAMS forecasts were also computed for observed wind speeds $\geq 1.5 \text{ m s}^{-1}$ in order to filter out errors associated with light and variable wind regimes. The bias, SD, and RMS error using this minimum wind-speed threshold are given by the dashed lines in Figure 9b2-4. The bias curve changes very little; however, both the SD and RMS errors decrease by as much as 15°, especially in the 3–12-h forecasts (0300 UTC to 1200 UTC) when light wind regimes dominate during the nocturnal and early morning hours. Nearly all of the decrease in the RMS error plot is associated with the decrease in the error SD. Thus, with wind speeds of at least 1.5 m s^{-1} , the maximum RMS error in the forecast wind direction is 50–60°, again primarily composed of non-systematic error.

Perhaps the most notable systematic error discovered in ERDAS RAMS is a predominant cool temperature bias that occurs during the daylight hours (Figure 9c). The cool bias develops after the 11-h forecast and continues for the remaining 13 hours of the forecast (Figure 9c2). The onset of the cool bias is closely juxtaposed with the time of sunrise. The average forecast temperature is nearly 4 °C too cool by the 18-h forecast (Figure 9c3-4). As a result, a significant portion of the RMS error is directly attributed to the inherent cool bias in the 12–24-h forecast (Figure 9c4).

Because the forecast temperatures were too cool and low-level moisture was simultaneously too high (not shown), it was hypothesized that the soil moisture was initialized too high. A sensitivity experiment was conducted in which the initial soil moisture was reduced by a factor of two. However, the results were very similar to the control simulation suggesting that soil moisture initialization is not the cause of the cool and moist bias at low-levels. The results presented in Snook et al. (1998) indicate a nearly identical pattern in the cool daytime temperature bias during real-time RAMS simulations over the southeastern United States in support of the 1996 summer Olympic games. Their sensitivity experiments suggest that RAMS is slow in mixing out the boundary layer during the late morning hours. In contrast, a recent study by Salvador et al. (1999) showed a warm daytime temperature bias in RAMS simulations at two coastal locations in Spain. Further investigation is necessary to isolate the possible cause(s) for the cool temperature bias in this warm-season study.

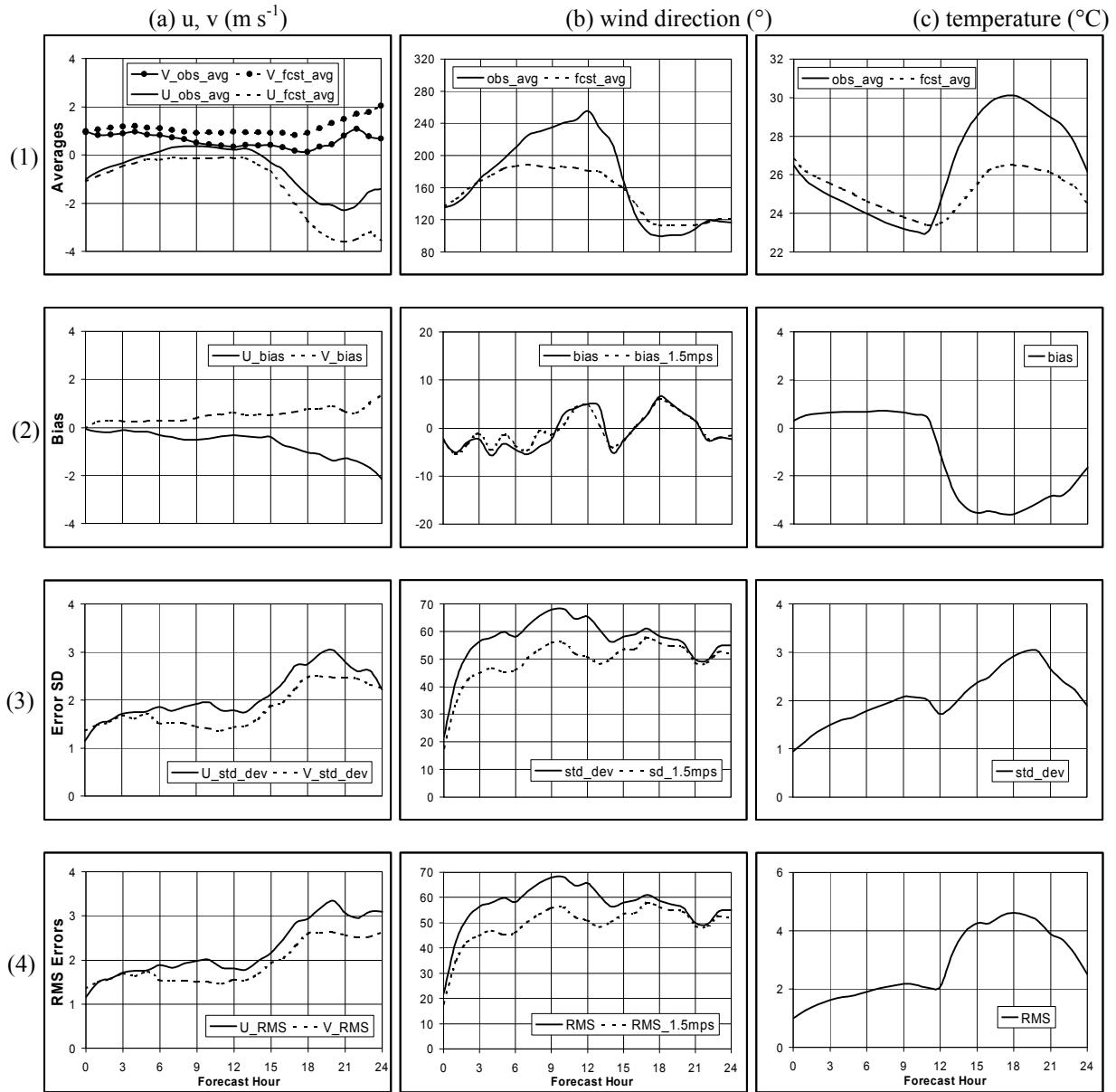


Figure 9. Average quantities, bias, error SD, and RMS error statistics are shown as a function of forecast hour for all valid warm-season (May–August) ERDAS RAMS forecasts initialized at 0000 UTC. Statistics are given for (a) u- and v-wind components (m s^{-1}), (b) wind direction ($^{\circ}$ from north), and (c) temperature ($^{\circ}\text{C}$). In (b), the bias, error SD, and RMS errors of wind direction are displayed for all data (solid line) and for only observations with wind speeds greater than 1.5 m s^{-1} (dashed line).

The warm-season error statistics for the 1200 UTC ERDAS RAMS runs are shown in Figure 10. Many of the same patterns occur as in the 0000 UTC error plots, except shifted by about 12 h. The cool temperature bias is also prevalent in the 1200 UTC ERDAS RAMS forecasts, but to a lesser extent than in the 0000 UTC forecasts. The maximum cool bias of -2.5 °C occurs at the 10-h forecast, then gradually approaches 0 °C by the 21-h forecast. However, the cool bias quickly redevelops between 23–24 h as average observed temperatures begin to rise whereas the forecast temperatures continue to cool slightly (Figure 10c1-2). The magnitude of the error SD from the 1200 UTC forecasts is about the same as in the 0000 UTC forecasts, but the maximum RMS errors from the 1200 UTC forecasts are about 1 °C smaller than the 0000 UTC forecasts due to the decrease in magnitude of the bias (Figs. 9c3-4 and 10c3-4).

Subjective verification of sea-breeze

The results from the subjective verification of the central Florida ECSB are summarized in Tables 12 and 13. A contingency table of the forecast and observed occurrences of the ECSB provides a summary of the model hits and misses along with the resulting categorical and skill scores (Table 12). No information on the timing of the ECSB is included in Table 13. This contingency table strictly focuses on the occurrence of the forecast and observed ECSB for a given forecast run and on a given day as described in the methodology. The maximum possible number of data points for Table 12 is 170 (2 forecasts per day \times 85 possible working days). However, only 135 samples were compiled due to system failures, deficient or missing Eta data, and employee absences.

The results from Table 12 suggest that ERDAS RAMS does an excellent job in forecasting the occurrence of the central Florida ECSB on grid 4. The high probability of detection (0.95) and critical success index (0.92) combined with a low false alarm ratio (0.03) strongly support this claim. The Heidke skill score (HSS) provides a benchmark of the model performance compared to pure chance (HSS=0). Thus, the HSS of 0.74 (Table 12) suggests that ERDAS RAMS forecasts of the ECSB provide a significant amount of improvement over random forecasts.

A summary of the forecast ECSB timing errors is given in Table 13 for the 0000 UTC and 1200 UTC ERDAS RAMS runs, and for all runs collectively. ERDAS RAMS output is available only once per hour, thus the verification of the ECSB timing at each KSC/CCAS tower is limited to the nearest hour. Despite this limitation, the results shown in Table 13 are quite good. The mean absolute error, RMS error, and standard deviation are all on the order of 1 h, whereas the bias is close to zero for both the 0000 UTC and 1200 UTC forecasts. The error statistics at each individual KSC/CCAS tower (not shown) do not indicate a correlation of timing errors and spatial location with respect to the coastline. Thus, the timing errors do not suggest a bias over any particular portion of the verification domain in Figure 8.

The subjective verification of the sea-breeze timing closely corresponds to the objective statistics. As shown in Figures 9 and 10, the forecast trends of the average wind direction, u-wind, and v-wind components closely match the observed trends. The small RMS errors and negligible bias in Table 13 indicate that on average, the timing of the forecast ECSB is quite accurate. Collectively, the objective and subjective verification statistics suggest that ERDAS RAMS provided a reliable and robust forecast of the onset and propagation of the central Florida ECSB during the 1999 warm season across the limited domain shown in Figure 8.

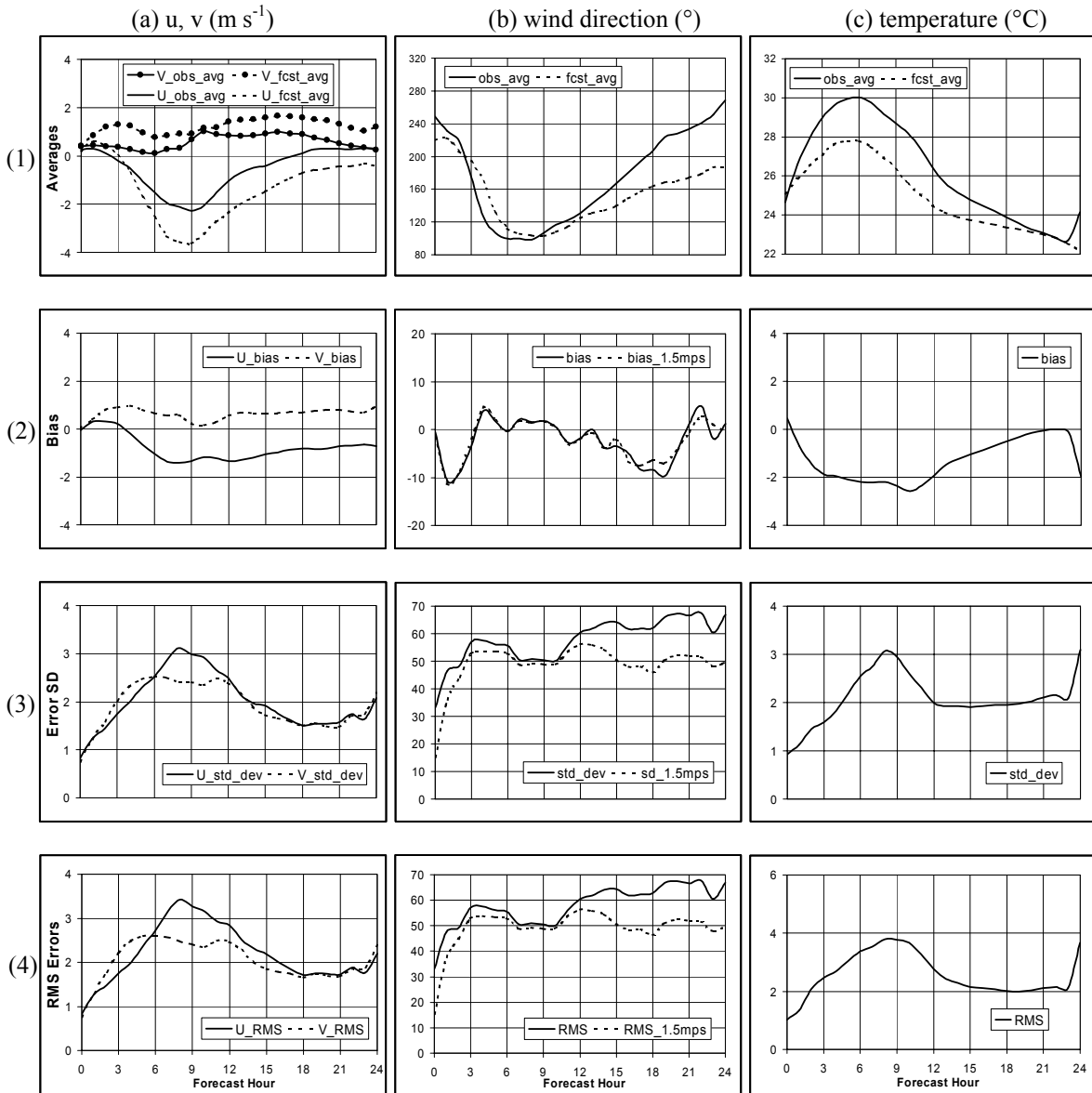


Figure 10. Average quantities, bias, error SD, and RMS error statistics are shown as a function of forecast hour for all valid warm-season (May–August) ERDAS RAMS forecasts initialized at 1200 UTC. Statistics are given for (a) u- and v-wind components ($m s^{-1}$), (b) wind direction ($^{\circ}$ from north), and (c) temperature ($^{\circ}C$). In (b), the bias, error SD, and RMS errors of wind direction are displayed for all data (solid line) and for only observations with wind speeds greater than $1.5 m s^{-1}$ (dashed line).

Table 12. Contingency table of the occurrence of ERDAS RAMS forecast sea breeze versus the observed sea breeze over east-central Florida. Corresponding skill scores are listed below.

	Observed Sea Breeze	No Observed Sea Breeze
Forecast Sea Breeze	110	3
Sea Breeze Not Forecast	6	16

Probability of Detection: 0.95 False Alarm Ratio: 0.03
 Critical Success Index: 0.92 Heidke Skill Score: 0.74

Table 13. A summary of error statistics for the May–August 1999 evaluation period are given for the subjective sea-breeze timing verification performed on the 13 KSC/CCAS tower locations in Figure 8. The mean absolute error (MAE), root mean square (RMS) error, standard deviation (SD), and bias are shown in units of hours for the 0000 UTC and 1200 UTC forecast runs, and for all runs collectively.

	0000 UTC	1200 UTC	All
MAE (h)	0.9	0.9	0.9
RMS (h)	1.3	1.3	1.3
SD (h)	1.3	1.3	1.3
Bias (h)	-0.2	0.1	0.0

Summary

The AMU evaluated the performance of real-time ERDAS RAMS forecasts during the 1999 Florida warm season months of May–August. The verification technique included both an objective and subjective component to determine the accuracy of ERDAS RAMS forecast winds, temperatures, and sea-breeze propagation on the inner-most nested grid centered on the KSC/CCAS.

Preliminary results from the objective verification indicate that up to a 2 m s⁻¹ easterly and a 1 m s⁻¹ southerly bias in the wind components occurred especially during times following the sea-breeze passage. Consequently, wind speeds were slightly too strong on average following the sea-breeze passage. Forecast wind direction was virtually unbiased and thus, non-systematic, random errors composed most of the total model error in forecast wind direction. This non-systematic error decreased by nearly 15° when calculating wind direction errors using a 1.5-m s⁻¹ minimum wind speed threshold. The most notable systematic error introduced by the model is a cool temperature bias (up to 4 °C in the 0000 UTC forecasts) that occurred during the daylight hours.

The subjective verification showed that ERDAS RAMS did an excellent job in forecasting the onset and movement of the ECSB. The timing errors associated with the forecast ECSB were on the order of 1 h suggesting that ERDAS RAMS performed quite well in predicting the onset and propagation of the ECSB during the 1999 warm season over the limited observational network in east-central Florida.

Future analysis of the 1999 warm-season error statistics will include examining histograms of the forecast errors to identify the favored modes of ERDAS RAMS errors. Also, forecast and observed data pairs at each evaluation tower will be examined for potential outliers in the data set. Statistics such as RMS error can be magnified by a few extreme errors. Therefore, more rigorous quality control of both the observational and forecast data will be applied in order to remove outliers and obtain the most representative quantification of ERDAS RAMS errors.

Future work in verifying real-time ERDAS RAMS forecasts also includes an evaluation of the model performance in predicting cold fronts, precipitation, temperatures, and winds during the 1999-2000 Florida cool season. An additional warm-season evaluation will be conducted during the summer months of 2000. Furthermore, future evaluations will be stratified into specific weather and model-error regimes to determine the strengths and weaknesses of ERDAS RAMS forecasts under specific meteorological conditions.

References

- Cetola, J. D., 1997: A Climatology of the sea breeze at Cape Canaveral, Florida. M. S. Thesis, Florida State University, Tallahassee, FL, 56 pp.
- Chen, S., and W. R. Cotton, 1988: The sensitivity of a simulated extratropical mesoscale convective system to longwave radiation and ice-phase microphysics. *J. Atmos. Sci.*, **45**, 3897-3910.
- Cotton, W. R., M. A. Stephens, T. Nehr Korn, and G. J. Tripoli, 1982: The Colorado State University three-dimensional cloud/mesoscale model — 1982. Part II: An ice phase parameterization. *J. de Rech. Atmos.*, **16**, 295-320.
- Davies, H. C., 1983: Limitations of some common lateral boundary schemes used in regional NWP models. *Mon. Wea. Rev.*, **111**, 1002-1012.
- Doswell, C. A., R. Davies-Jones, and D. Keller, 1990: On summary measures of skill in rare event forecasting based on contingency tables. *Wea. Forecasting*, **5**, 576-585.
- Lyons, W. A., and C. J. Tremback, 1994: Predicting 3-D wind flows at Cape Canaveral Air Force Station using a mesoscale model. Contract No. F04701-91-C-0058, Los Angeles AFB, CA, 592 pp. [Available from United States Air Force, Space and Missile Systems Center, SMC/CLNE, Los Angeles AFB, CA 90245-4683].
- Mellor, G. L., and T. Yamada, 1982: Development of a turbulence closure model for geophysical fluid problems. *Rev. Geophys. Space Phys.*, **20**, 851-875.
- Merceret, F. J., 1995: The effect of sensor sheltering and averaging techniques on wind measurements at the Shuttle Landing Facility. NASA Technical Memorandum TM-111262, 42 pp. [Available from NASA Center for Aerospace Information, 7121 Standard Dr., Hanover, MD, 21076-1320.]
- Pielke, R. A., W. R. Cotton, R. L. Walko, C. J. Tremback, W. A. Lyons, L. D. Grasso, M. E. Nicholls, M. D. Morgan, D. A. Wesley, T. J. Lee, and J. H. Copeland, 1992: A comprehensive meteorological modeling system — RAMS. *Meteorol. Atmos. Phys.*, **49**, 69-91.
- Salvador, R., J. Calbó, and M. Millán, 1999: Horizontal grid size selection and its influence on mesoscale model simulations. *J. Appl. Meteor.*, **38**, 1311-1329.
- Schaefer, J. T., 1990: The critical success index as an indicator of warning skill. *Wea. Forecasting*, **5**, 570-575.
- Snook, J. S., P. A. Stamus, and J. Edwards, 1998: Local-domain analysis and forecast model support for the 1996 Centennial Olympic Games. *Wea. Forecasting*, **13**, 138-150.
- Tremback, C. J., 1990: Numerical simulation of a mesoscale convective complex: model development and numerical results. Ph.D. Dissertation, Atmos. Sci. Paper No. 465, Department of Atmospheric Science, Colorado State University, Fort Collins, CO 80523, 247 pp.
- Tremback, C. J., and R. Kessler, 1985: A surface temperature and moisture parameterization for use in mesoscale numerical models. *Preprints, 7th AMS Conf. on Numerical Weather Prediction*, June 17-20, Montreal, Quebec, Amer. Meteor. Soc., Boston, MA, 355-358.

Turner, D. B., 1986: Comparison of three methods for calculating the standard deviation of the wind direction. *J. Climate Appl. Meteor.*, **25**, 703-707.

SUBTASK 9 LOCAL DATA INTEGRATION SYSTEM EXTENSION (MR. CASE)

During the past quarter, Mr. Case wrote the first draft of the final report entitled Simulation of a Real-Time Local Data Integration System (hereafter LDIS Phase II). The LDIS Phase II final report describes the methodology in archiving a real-time data set, the modified configuration for the simulated real-time LDIS, sample case studies, and the sensitivities and deficiencies encountered. Also, hardware and software recommendations are provided for customer implementation of a real-time LDIS at a particular office.

In this quarterly report, a subset of the LDIS Phase II final report is provided. The discussion includes the modified task plan, data archiving methodology, configuration for the simulated real-time LDIS and modifications from LDIS Phase I, and the hardware recommendations for running LDIS in real-time.

Introduction

Results from the AMU report entitled Final Report on Prototype Local Data Integration System and Central Florida Data Deficiency (Case and Manobianco 1998, hereafter LDIS Phase I) show that much utility can be gained by running a high-resolution mesoscale analysis system. LDIS Phase II extends the LDIS Phase I efforts by describing the utility of a simulated real-time LDIS and examining the sensitivities and deficiencies related to such a configuration. The LDIS Phase II report provides SMG, 45 WS, and the NWS MLB with information on the utility of a real-time LDIS, the hardware necessary to run LDIS in real-time, the strengths and weaknesses of a real-time LDIS, and additional steps that may be required to implement a real-time LDIS at a particular office.

Initial Task Objectives

As written in the original task proposal, the objectives for LDIS Phase II were as follows.

- Optimize temporal continuity of the analyses especially for cloud parameters.
- Determine if any modifications are required to run the prototype configuration in real-time on available hardware.
- Simulate real-time LDIS runs using available real-time data for a period of 1-2 weeks.
- Determine the deficiencies and/or sensitivities of the simulated real-time configuration from the additional case studies and suggest and/or test improvements and/or fixes.

Modifications to Original Task Plan

The original task objectives were modified slightly based on consensus from a teleconference that took place during January 1999. Because the AMU identified that the primary cause for temporal discontinuities was the presence or absence of various contributing data sources in successive analyses, all customers agreed that little additional time should be spent on improving the temporal continuity of analyzed variables. Instead, the AMU should identify the data types that cause observed discontinuities so that operational forecasters can recognize the influence of specific data sets on LDIS.

It was also determined at this teleconference that the AMU should continue using the Advanced Regional Prediction System (ARPS) Data Analysis System (ADAS) software on the same hardware platform as used in LDIS Phase I. The LDIS Phase II task utilizes the same hardware and software for two reasons. First, an extensive amount of time would be required to reinstall ADAS on different hardware or to change analysis software packages. Second, the customers are most interested in determining the hardware necessary to run LDIS in real-time with minimal modifications from the Phase I configuration. Therefore, no modifications to the LDIS Phase I configuration were suggested. Instead, the performance of LDIS on the existing hardware is evaluated. If LDIS run-time on the existing hardware is inadequate for real-time, then the AMU will estimate the hardware specifications necessary to run LDIS in real-time.

The results from LDIS Phase I indicate that WSR-88D data contribute significantly toward the analysis of winds and clouds. However, level II WSR-88D data from only the Melbourne site were used in LDIS Phase I whereas level III data are operationally available at SMG for all Florida sites. Level III data consists of reflectivity and radial velocity observations at a slightly degraded horizontal resolution for only the lowest four elevation angles. Therefore, one important issue for LDIS Phase II is to compare the influence of level II versus level III WSR-88D data on the subsequent ADAS analyses. The comparison addresses the impact of using level II versus level III data and the possible benefits in the analyses by using level III data from multiple WSR-88D sites.

The updated and final LDIS Phase II task objectives are as follows.

- Simulate a real-time LDIS using available real-time data for a period of 2 weeks.
- Identify the data types that cause observed discontinuities so LDIS users can recognize the data influences.
- Evaluate system performance on existing hardware and extrapolate the performance to determine the hardware necessary to run a real-time LDIS.
- Determine the sensitivities and/or deficiencies of the simulated real-time configuration from additional case studies and suggest and/or test improvements and/or fixes.

Methodology

An appropriate data archiving strategy must be adopted to obtain an optimal two-week data set for the real-time LDIS simulation. Once the optimal data set is selected, several modifications to the data ingestors and LDIS configuration are necessary in order to simulate a real-time configuration. This section describes the data archiving procedures used in LDIS Phase II, outlines the aspects of the LDIS configuration that remained the same as in LDIS Phase I, and addresses the portions of the LDIS configuration that were modified for the real-time simulation.

Selection of Real-time Data Set

The two-week real-time data archive used in LDIS Phase II is 15-28 February 1999. During a January 1999 teleconference involving the AMU, SMG, 45 WS, and NWS MLB, a methodology was established to select an optimal two-week period in which the AMU could simulate and evaluate the performance of a real-time LDIS configuration. The methodology includes the strategy used to select the optimal data set and data archiving procedures.

The methodology for selecting the optimal two-week data set is as follows.

- A continuous data archive was saved for at least a two-week period at both SMG and NWS MLB.
- If an insufficient number of case study days were available due to benign weather during the first two-week time period, then the subsequent two-week period was archived.
- This process persisted until the most suitable two-week data set was archived. A final date (1 April) for the data archiving window was chosen to provide the AMU with sufficient time for running LDIS and analyzing the output, sensitivities, and deficiencies.

The following organizations performed data archiving.

- NWS MLB archived all Melbourne level II WSR-88D data.

- The AMU downloaded Aeronautical Radio, Inc. (ARINC) Communications, Addressing and Reporting System (ACARS) data from the Forecasts Systems Laboratory (FSL) web site (<http://acweb.fsl.noaa.gov>; Schwartz and Benjamin 1995). ACARS data consist of automated aircraft observations of temperature and winds and can provide valuable soundings during aircraft ascents and descents.
- All other data were archived at SMG and sent to the AMU for real-time LDIS simulations. These data were saved directly from their real-time sources and include GOES-8 visible (VIS) and infrared (IR) imagery, level III WSR-88D data for all Florida radar sites, Rapid Update Cycle (RUC) model 0-, 3-, and 6-h forecast grids, and all textual and point data from the Meteorological Interactive Data Display System (MIDDS).

Unmodified LDIS Configuration

Analysis Software

As in LDIS Phase I, the AMU used the ADAS software available from the Center for Analysis and Prediction of Storms (CAPS) in Norman, OK (Brewster 1996). ADAS utilizes the Bratseth objective analysis procedure (Bratseth 1986) consisting of an iterative successive corrections method (SCM, Bergthorsson and Doos 1955) that converges to the statistical or optimum interpolation (OI). Generally, OI is superior to SCM because OI accounts for variations in data density, observational errors, and accounts for dynamical relationships between variables such as wind and pressure. The Bratseth scheme realizes the advantages of OI while retaining the computational efficiency of SCM. The LDIS Phase I report provides a detailed description of the objective analysis algorithm, the complex cloud scheme (CCS), and QC procedures associated with ADAS.

ADAS analyzes five variables at each model vertical level: u- and v-wind components, pressure, potential temperature, and RH*. RH* is a moisture variable analogous to dew-point depression and is defined as:

$$RH^* = \sqrt{1.0 - RH},$$

where RH is the relative humidity. The ARPS/ADAS vertical coordinate is a terrain-following height coordinate analogous to the traditional sigma coordinate.

Nested Grid Configuration

The same nested grid configuration is retained as in LDIS Phase I following the Integrated Terminal Weather System (ITWS; Cole and Wilson 1995). ADAS is run every 15 minutes at 0, 15, 30, and 45 minutes past the hour over outer and inner grids with horizontal resolutions of 10-km and 2-km respectively. The RUC model is used as a background field for the 10-km ADAS analysis and the resulting 10-km analysis is used as a background field for the 2-km analysis. RUC forecasts are received in real-time at SMG interpolated to an 80-km grid with vertical levels every 50 mb from 1000–100 mb. RUC data are linearly interpolated in time every 15 minutes for each 10-km analysis cycle. The 10-km (2-km) analysis grid covers an area of 500 × 500 km (200 × 200 km) and contains 30 vertical levels that extend from near the surface to about 16.5 km above ground level. The terrain-following vertical coordinate is stretched such that the finest resolution (20 m) occurs near the ground whereas the coarsest resolution (~ 1.8 km) occurs at the top of the domain. The horizontal coverage and grid-point distributions for both the 10-km and 2-km analysis grids are shown in Figure 11.

Data Ingest Window

The data ingest strategy from LDIS Phase I is retained for the real-time simulation in the current study. Data are ingested at times closest to the valid analysis time within a 15-minute window centered on the analysis time (± 7.5 minutes). In this possible real-time configuration, data ingest would start each cycle after the actual analysis time to allow for the transmission, receipt, and processing of real-time data. This particular strategy is retained for the current study because each analysis cycle consists of observations grouped as closely together in time making the analysis as representative as possible. An alternative data ingest configuration is to start each cycle at the actual analysis time and incorporate all data collected since the previous cycle. However, this data ingest configuration

could result in a less representative mesoscale analysis because observational data would be spaced farther apart in time. Moreover, extensive modifications would have been required to update the data ingest programs for this alternative strategy.

Also as in LDIS Phase I, GOES-8 IR and VIS brightness temperature data in an image format are converted/remapped to both the 10-km and 2-km analysis grids every 15 minutes. The brightness temperature data are then used in the CCS of ADAS to derive various cloud fields.

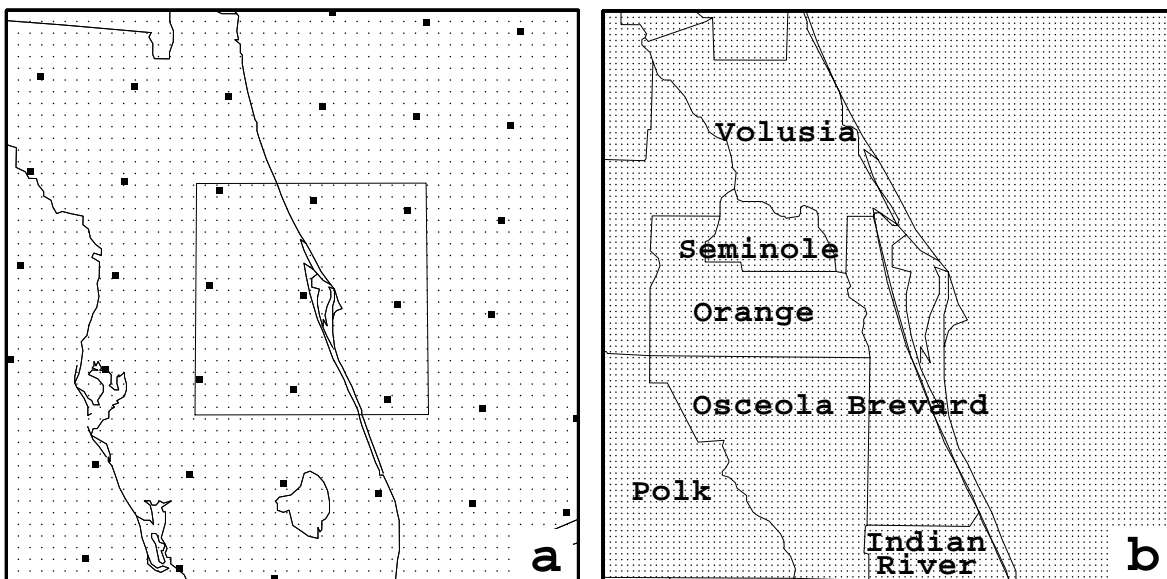


Figure 11. The ADAS domains for the 10-km grid and 2-km grid are depicted in panels a) and b), respectively. The 10-km grid point (small dots) and 80-km RUC grid point locations (solid squares) are shown in panel a) while the 2-km grid point locations (small dots) and county labels are shown in panel b). The boxed region in panel a) denotes the 2-km domain.

Modifications for the Simulated Real-time Configuration

Several modifications to the data ingestors were required in order to appropriately simulate a real-time LDIS configuration. Instead of working with idealized data sets obtained after the fact as in LDIS Phase I, the data archived in real-time are ingested as received into ADAS. Therefore, new issues to address include missing data, data latency between observation and receipt times, and limitations of the available real-time data sets.

Background field

As in LDIS Phase I, the RUC model (Benjamin et al. 1998) is used as a background field for the subsequent 10-km ADAS analyses. However, the RUC data received at SMG have a horizontal resolution of 80 km and a vertical resolution of 50 mb whereas 40-km and 60-km RUC data at 25-mb intervals were used in LDIS Phase I. Furthermore, because the real-time RUC data are received at SMG up to 3 hours after the model initialization time (Table 14), RUC 3–6-h forecasts rather than analyses are used as background fields for ADAS.

While converting these RUC data onto the 10-km analysis grid, there are specific times when RUC forecasts are missing from the data archive (not shown). Correspondingly, no ADAS analyses are generated for times when RUC data are not available. This problem could be ameliorated by using older RUC forecast grids (6–12-h forecasts) and/or Eta model forecast grids as a background field for ADAS. However, these options were not feasible in LDIS Phase II because only the RUC 0–6-h forecasts were archived.

Table 14. Real-time data source and estimation of real-time data latency from observation time to receipt time at SMG.

Data Type	Real-Time Source	Time Lag
Surface Observations (METAR)	MIDDS	10 min
Ship/Buoy	MIDDS	10 min
KSC/CCAS Towers	MIDDS	1-2 min
National Rawinsondes	MIDDS	≥ 2.0 h
Cape Canaveral Rawinsonde	MIDDS	20 min
ACARS	NOAA FSL	15 min ¹
PIREPS	MIDDS	5-30 min ²
GOES-8 VIS/IR	MIDDS	5 min
GOES-8 Soundings	MIDDS	50 min
GOES-8 derived winds	MIDDS	2.0 h
915 MHz profilers	MIDDS	1-2 min
50 MHz profiler	MIDDS	1-2 min
Level II WSR-88D	NWS MLB	< 1 min ³
Level III WSR-88D	MIDDS	3-5 min
80-km RUC forecast	MIDDS	2.5-3.0 h

¹Estimated for FSL data.

²Estimated for 45 WS data.

³NWS MLB office only (Sharp 1999, personal communication).

Real-time Data

As indicated in Table 14, all real-time data sources except ACARS and level II WSR-88D data are available and archived through MIDDS. ADAS reads data in a text format for ingest into the analysis cycle. All the point/textual data available through MIDDS are converted to ASCII format by accessing Man-computer Interactive Data Access System for UNIX (McIDAS-X) programs non-interactively and preparing the textual data for ingest into ADAS. ACARS data were recently made available in real-time from FSL by means of a local data management feed. Level II WSR-88D data are available in real-time only at NWS MLB.

Due to limitations in their current communication line bandwidth, SMG cannot receive the full-volume level II WSR-88D data in real-time. SMG currently receives level III WSR-88D products in real-time from a NEXRAD (NEXt generation RADar) Information Dissemination Service (NIDS) vendor. The products currently available from SMG's NIDS vendor include reflectivity and radial velocity data for the four lowest elevation angles at the MLB WSR-88D site, and the two lowest elevation angles at all other Florida radar sites (Tallahassee, TLH; Jacksonville, JAX; Tampa Bay, TBW; Miami, AMX; and Key West, EYW).

The format of the level III reflectivity and radial velocity products required several modifications to the existing radar conversion/remapping program of ADAS. The existing ADAS remapping program reads WSR-88D level III data from its hybrid coordinates: azimuth, range, and elevation angle. However, the level III products received at SMG are stored on a quasi-horizontal coordinate system (x, y, and elevation angle). Therefore, one of the significant modifications to the remapping program is to identify a common spatial position relative to the WSR-88D radar site. In this instance, latitude, longitude, and height served as the common thread between the two coordinate systems. Once the data positions are identified, the reflectivity and radial velocity data are converted to the analysis grid for ingest into the ADAS algorithms.

The most substantial change in the spatial distribution of the real-time radar data compared to the radar data used in LDIS Phase I is the increased horizontal coverage on the 10-km analysis domain. In LDIS Phase I, only the MLB WSR-88D data were used and its horizontal coverage is given by the dark shaded region in Figure 12a. However, the horizontal coverage of all the radar sites used in LDIS Phase II is denoted by the areas of light and dark shading collectively in Figure 12a. The locations of the MLB WSR-88D and the KSC/CCAS data on the 2-km analysis grid are shown in Figure 12b.

The MLB WSR-88D influences all of the 2-km domain and a large portion of the 10-km domain (Figure 12a). However, several other Florida radar sites also influence large portions of the 10-km domain (TLH, JAX, TBW, and AMX) and even the 2-km domain (TBW and JAX). Because each level III WSR-88D data set has a range of 230 km, the additive effect of all radar sites results in nearly continuous horizontal coverage of reflectivity and radial velocity data at low-levels on the 10-km and 2-km analysis grids.

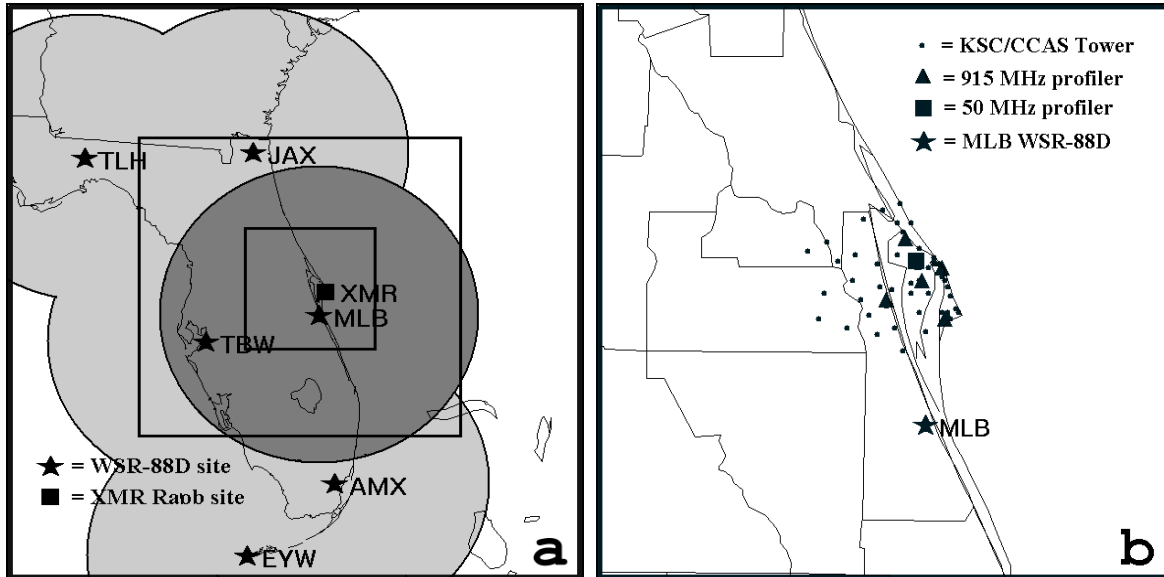


Figure 12. The distribution of WSR-88D data and KSC/CCAS observations in the simulated real-time configuration are shown over the Florida peninsula and the 2-km analysis grids respectively. The dark shading in a) represents the areal coverage of the Melbourne WSR-88D whereas the light and dark shading collectively represent the areal coverage of all Florida radar sites. Outlines of the 10-km (outer) and 2-km (inner) analysis domains and the location of the Cape Canaveral (XMR) rawinsonde also given in a). The locations of the KSC/CCAS towers, 915 MHz and 50 MHz profilers, and the Melbourne WSR-88D are shown in b).

Data Latency

An important issue to consider when configuring LDIS is the lag that occurs between the time of observation and the time that the data are received at a local office. The type and amount of data that should be ingested largely depend on the scales of motion to be sampled and the cycle time of the integration system. Because LDIS is designed to provide mesoscale analyses at 15-minute intervals, the most valuable real-time data sources provide observations at least as often as the analysis cycle. However, if data that experience large time lags are ingested into ADAS as soon as the observations become available, then outdated information could be incorporated especially during rapidly-evolving mesoscale weather such as deep convection and outflow boundaries.

Table 14 provides a summary of the estimated time lags for each real-time data source as received locally at SMG (Oram 1999, personal communication). The AMU identified three data sources with substantial time lags and excluded these data from the real-time LDIS simulation based on several considerations.

- According to the time lags in the third column of Table 14, national rawinsondes (2 h), GOES-8 derived winds (2 h), and GOES-8 soundings (50 min) experience time lags significantly longer than the cycle time for LDIS (15 min).
- ADAS does not currently have the capability to time-weight observational data as in the data assimilation systems currently used in the national-scale operational models (such as the RUC and Eta).

- The Local Analysis and Prediction System (LAPS) was run operationally to provide weather support for the 1996 summer Olympic games. LAPS generated surface (upper-air) analyses every 15 (30) minutes across the southeastern United States at a horizontal resolution of 8 km. In the LAPS real-time configuration, data with large time lags such as rawinsondes were not ingested (Snook et al. 1998).
- National rawinsondes and GOES-8 derived winds are currently ingested into the RUC hourly data assimilation cycle (Benjamin and Brundage 1999). Therefore, these two data sources already have an indirect impact on the ADAS analyses through the RUC background fields.

Summary of LDIS Configuration Modifications

Table 15 provides a summary of the analysis configuration in LDIS Phase I versus Phase II. The primary configuration changes for the real-time simulations include the following.

- Use of 80-km RUC 3–6-h forecasts as background fields for the 10-km ADAS analysis.
- Exclusion of data sources with large time lags compared to the analysis cycle (Florida rawinsonde sites except the Cape Canaveral site, GOES-8 derived winds, and GOES-8 soundings).
- Use of level III WSR-88D data from all Florida radar sites.

Table 15. Comparison between the analysis configuration in LDIS Phase I versus Phase II.		
Configuration	LDIS Phase I	LDIS Phase II
Software	ADAS	ADAS
Hardware	IBM RS/6000	IBM RS/6000; HP (graphics)
Grid	10-km, 2-km nest	10-km, 2-km nest
Cycle frequency	Every 15 minutes on 1/4 hour	Every 15 minutes on 1/4 hour
Data ingest	± 7.5 minutes	± 7.5 minutes
Background field	40-km, 60-km RUC 0-h forecasts	80-km RUC 3–6-h forecasts
Point/Text data	Ingests all data sources	Excludes data with large time lags
Satellite data	GOES-8 IR/VIS	GOES-8 IR/VIS
WSR-88D data	Level II, MLB only	Level III, all FL sites

Hardware and System Performance

This section describes some fundamental hardware characteristics for the AMU workstation used to simulate the real-time LDIS runs. The discussion includes a documentation of system performance for the two-week simulation, the real-time requirements for SMG, and estimated hardware characteristics for a workstation necessary to run LDIS in real-time.

Hardware used

The AMU ran the ADAS analysis cycle on an International Business Machine (IBM) RS/6000, machine type 7012, model 390 workstation. This workstation contains a 67-MHz clock rate and a PWR2 chip. Allocated memory is maximized on this machine at 512 megabytes (MB) whereas the standard memory with this workstation is only 32 MB. The 512 MB of memory is necessary to run ADAS because the 2-km analysis program is run on a 100x100x30 grid and requires 267 MB of memory. All other ADAS programs within the analysis cycle require less memory.

For post-processing, the AMU ran various General Meteorological Package (GEMPAK) programs to generate graphical display products for qualitative examination. In order to complete the two-week simulation in a reasonable time frame, all graphics were generated on a separate HP workstation in conjunction with the ADAS analysis cycle on the IBM machine. However, since specific graphical products are so highly dependent on the operational needs of each individual office, the run-time performance of the graphical programs are not discussed.

Run-time Performance

All programs involved in the ADAS analysis cycle and their corresponding wall-clock times are given in Table 16. The ADAS cycle is composed of several programs for creating the analyses, interpolation, and conversion to GEMPAK format. First, RUC variables on pressure coordinates are interpolated to the ADAS 10-km grid. The 10-km ADAS analysis is then performed and the resulting data are converted to GEMPAK format for post-processing. The 10-km ADAS cloud products (cloud-top heights, ceilings, and cloud fraction) are also converted to GEMPAK format. Another conversion program interpolates the 10-km analysis data to the 2-km ADAS grid. Following this interpolation, the 2-km analysis is performed followed by a conversion to GEMPAK format. Finally, the 2-km cloud analysis products are converted to GEMPAK format.

The mean wall-clock time of each program in the ADAS cycle indicates that the current analysis configuration runs in real-time on the AMU's IBM RS/6000 workstation. The ADAS analysis cycle averages 7.29 min for all cycles in the two-week simulation period (Table 16). Given that the analysis cycle completes every 15 minutes, the current configuration on the AMU workstation runs faster than real-time, but does not include data pre-processing and graphical post-processing times.

Table 16. The mean and standard deviations of wall clock run-times for each program in the ADAS analysis cycle are given along with the total cycle time. These times are valid for the IBM RS/6000 UNIX workstation in the AMU lab and do not include data ingest, conversion, and post-processing times for graphics production.		
ADAS Program	Mean Wall Clock Time (min)	Standard Deviation (min)
RUC to 10-km grid conversion	0.48	0.04
10-km ADAS	1.28	0.07
10-km to 2-km grid conversion	2.20	0.38
2-km ADAS	3.33	0.64
Total Wall Clock Time	7.29	----

Estimation of Hardware Required for Real-time

In an operational mode, the 7.29-minute cycle wall-clock time on the AMU workstation is not sufficient because data preparation, analysis computations, and graphical post-processing should all be completed within about 5 minutes of the analysis window according to SMG specifications. SMG determined this 5-minute constraint based on the need to obtain operational analysis products in a timely fashion. This constraint requires a workstation that can complete the analysis cycle approximately three times faster than the IBM RS/6000 machine used in this study. Because all facets of computer hardware have improved over the past several years since the AMU acquired the IBM RS/6000 machine, it is difficult to address the exact specifications required to run the ADAS cycle in a given amount of time. Besides increasing the central processing unit (CPU) speed, several other factors will also reduce the wall-clock time including improved input/output capabilities with new hard disk drives and improved network connections.

By focusing on just the CPU speed and no other factors, a workstation with a 200-MHz processor should be sufficient to run the ADAS cycle about three times faster than the IBM workstation used in this study. Furthermore, increased efficiency can be obtained by utilizing a workstation with multiple processors. For example, a two-processor workstation at 200-MHz CPU speed per processor would run faster than a single processor workstation with the same CPU rating. Also, the maximum memory used by any of the ADAS programs is 267 MB. Therefore, the memory of the workstation must exceed 267 MB and the AMU suggests at least 512 MB of memory on a

workstation used for a real-time LDIS.

Two other aspects of the real-time LDIS are the preparation of all data sources for ingestion into ADAS and the post-processing of graphical analysis products. A good strategy for data preparation could be to run all data converters on a separate workstation connected to the same network as the LDIS workstation. In this study, most of the real-time point and text data are prepared for ADAS using McIDAS-X programs (version 7.501). Therefore, the pre-processing workstation must accommodate McIDAS-X version 7.5 or higher which utilizes the Abstract Data Distribution Environment (ADDE) format. GOES-8 imagery and WSR-88D data are remapped onto the analysis grids and therefore require extra wall-clock time in addition to the ADAS analysis cycle (not shown). In general, the wall-clock times for data ingestion are relatively negligible compared to the actual analysis and interpolation programs. If the workstation used for a real-time LDIS has a sufficiently fast processor speed, then it could be used for running the data ingestors, the ADAS analysis cycle, and graphical post-processing. However, the data ingestors and graphical post-processing could also be run on a separate workstation whereas the LDIS workstation is dedicated to the analysis cycle given in Table 16. By running on two separate workstations, the machine dedicated to the ADAS cycle will not require such a fast processor, and thus will not be as expensive.

References

- Benjamin, S. G., J. M. Brown, K. J. Brundage, D. Devenyi, B. E. Schwartz, T. G. Smirnova, T. L. Smith, L. L. Morone, and G. J. DiMego, 1998: The operational RUC-2. *16th Conf. on Weather Analysis and Forecasting*, Phoenix, AZ, Amer. Meteor. Soc., 249-252.
- Benjamin, S., and K. Brundage, FSL, cited 1999: MAPS/RUC Information. [Available on-line from <http://maps.fls.noaa.gov>.]
- Bergthorsson, P., and B. Doos, 1955: Numerical weather map analysis. *Tellus*, **7**, 329-340.
- Bratseth, A., 1986: Statistical interpolation by means of successive corrections. *Tellus*, **38A**, 439-447.
- Brewster, K., 1996: Application of a Bratseth analysis scheme including Doppler radar data. Preprints, *15th Conf. on Weather Analysis and Forecasting*, Norfolk, VA, Amer. Meteor. Soc., 92-95.
- Case, J. L., and J. Manobianco, 1998: Final report on prototype local data integration system and central Florida data deficiency. NASA Contractor Report CR-1998-208540, Kennedy Space Center, FL, 57 pp. [Available from ENSCO, Inc., 1980 N. Atlantic Ave., Suite 230, Cocoa Beach, FL 32931].
- Cole, R. E., and W. W. Wilson, 1995: ITWS gridded winds product. Preprints, *6th Conf. on Aviation Weather Systems*, Dallas, TX, Amer. Meteor. Soc., 384-388.
- Schwartz, B., and S. G. Benjamin, 1995: A comparison of temperature and wind measurements from ACARS-equipped aircraft and rawinsondes. *Wea. Forecasting*, **10**, 528-544.
- Snook, J. S., P. A. Stamus, and J. Edwards, 1998: Local-domain analysis and forecast model support for the 1996 Centennial Olympic Games. *Wea. Forecasting*, **13**, 138-150.

2.5 AMU CHIEF'S TECHNICAL ACTIVITIES (DR. MERCERET)

An article describing the results of Dr. Merceret's study of the lifetime of wind features as a function of their vertical size was submitted to the *Journal of Applied Meteorology* for publication. Dr. Merceret is consulting with the Space Shuttle program on the characteristics of wind flow around the Vehicle Assembly Building. He is also consulting with the Titan program on an error analysis of upper-air wind systems and with Boeing on the operational use of 50 MHz profiler data for Delta launches.

NOTICE

Mention of a copyrighted, trademarked, or proprietary product, service, or document does not constitute endorsement thereof by the author, ENSCO, Inc., the AMU, the National Aeronautics and Space Administration, or the United States Government. Any such mention is solely for the purpose of fully informing the reader of the resources used to conduct the work reported herein.

List of Acronyms

30 SW	30th Space Wing
30 WS	30th Weather Squadron
45 LG	45th Logistics Group
45 OG	45th Operations Group
45 SW	45th Space Wing
45 WS	45th Weather Squadron
ACARS	ARINC Communications, Addressing and Reporting System
ADAS	ARPS Data Assimilation System
ADDE	Abstract Data Distribution Environment
AFRL	Air Force Research Laboratory
AFSPC	Air Force Space Command
AFWA	Air Force Weather Agency
AMU	Applied Meteorology Unit
AMX	Miami, Florida
ARINC	Aeronautical Radio, Inc.
ARPS	Advanced Regional Prediction System
CAPS	Center for Analysis and Prediction of Storms
CCAS	Cape Canaveral Air Station
CCS	Complex Cloud Scheme
CPU	Central Processing Unit
CSR	Computer Sciences Raytheon
ECSB	East Coast Sea Breeze
EDA	Exploratory Data Analysis
ERDAS	Eastern Range Dispersion Assessment System
EYW	Key West, Florida
FC	False Cape 915 MHz Profiler
FSL	Forecast Systems Laboratory
FSU	Florida State University
FY	Fiscal Year
GEMPAK	General Meteorological Package
HP	Hewlett Packard
HSS	Heidke Skill Score
HYPACT	HYbrid Particle And Concentration Transport
I&M	Improvement and Modernization
IBM	International Business Machine
IFR	Instrument Flight Rules
JAX	Jacksonville, Florida
JSC	Johnson Space Center
KSC	Kennedy Space Center

List of Acronyms

LAN	Local Area Network
LAPS	Local Analysis and Prediction System
LDIS	Local Data Integration System
LIFR	Low Instrument Flight Rules
LR	Logistic Regression
LWO	Launch Weather Officer
MARSS	Meteorological And Range Safety Support
MB	Megabyte
McIDAS	Man-computer Interactive Data Access System
MHz	Mega-Hertz
MI	Merritt Island 915 MHz Profiler
MIDDS	Meteorological Interactive Data Display System
MLR	Multiple Linear Regression
MSFC	Marshall Space Flight Center
MVFR	Marginal Visual Flight Rules
NASA	National Aeronautics and Space Administration
NBS	NOAAPORT Broadcast System
NCAR	National Center for Atmospheric Research
NE	Northeast
NEXRAD	NEXt generation RADar
NIDS	NEXRAD Information Dissemination Service
NOAA	National Oceanic and Atmospheric Administration
NSSL	National Severe Storms Laboratory
NWS MLB	National Weather Service Melbourne
OK	Oklahoma
OI	Optimal Interpolation
POR	Period of Record
Q	Quality flag provided by sodar vendor
QC	Quality Control
RAMS	Regional Atmospheric Modeling System
RH	Relative Humidity
RMS	Root Mean Square
RSA	Range Standardization and Automation
RUC	Rapid Update Cycle
SBIR	Small Business Innovative Research
SCM	Successive Corrections Method
SD	Standard Deviation
SMC	Space and Missile Center
SMG	Spaceflight Meteorology Group

List of Acronyms

SNR	Signal to Noise Ratio
SOW	Statement Of Work
STS	Space Transportation System
TBW	Tampa Bay, Florida
TLH	Tallahassee, Florida
USAF	United States Air Force
UTC	Universal Coordinated Time
VFR	Visual Flight Rules
WSMR	White Sands Missile Range
WSR-88D	Weather Surveillance Radar - 88 Doppler
WWW	World Wide Web
Y2K	Year 2000

Appendix A

AMU Project Schedule 31 October 1999				
AMU Projects	Milestones	Actual / Projected Begin Date	Actual / Projected End Date	Notes/Status
Statistical Short-range Forecast Tools	Determine Predictand(s)	Aug 98	Sep 98	Completed
	Data Collection, Formulation and Method Selection	Sep 98	Apr 99	Completed
	Equation Development	Feb 99	Oct 99	Delayed – waiting for guidance from customers on how to proceed
	Tests with Independent Data	Apr 99	Oct 99	Await completion of eqn development
	Tests with Individual Cases	May 99	Oct 99	Await completion of eqn development
	Prepare Products, Final Report for Distribution	May 99	Nov 99	Await completion of eqn development
LDIS Extension	Optimize Temporal Continuity of Analyses	Oct 98	Dec 98	Completed
	Determine Configuration Changes Required for Simulated Real-time Runs	Nov 98	Feb 99	Completed
	Simulate Real-time Runs	Feb 99	May 99	Completed
	Determine Deficiencies /Sensitivities of Simulated Real- time Runs	Apr 99	Jun 99	Completed
	Final Report	May 99	Oct 99	Undergoing external review
Meso-Model Evaluation	Recommend Models for Evaluation	Jul 98	Dec 98	Completed
	Develop ERDAS/RAMS Evaluation Protocol	Feb 99	Mar 99	Completed
	Perform ERDAS/RAMS Evaluation	Apr 99	Sep 99	Completed
	Extend ERDAS/RAMS Evaluation	Oct 99	Sep 00	On Schedule
	Interim ERDAS/RAMS Report	Dec 99	Jan 00	On Schedule
	Final ERDAS/RAMS Report	Oct 00	Dec 00	On Schedule
Delta Explosion Analysis	Analyze Radar Imagery	Jun 97	Nov 97	Completed
	Run Models/Analyze Results	Jun 97	Jun 98	Completed
	Final Report	Feb 98	Oct 99	Ready for external review
	Launch site climatology plan	Apr 98	May 98	Completed

AMU Project Schedule

31 October 1999

AMU Projects	Milestones	Actual / Projected Begin Date	Actual / Projected End Date	Notes/Status
Evaluation of Sodar Wind Profiler	Collect Data	Apr 99	May 99	Completed
	Perform Evaluation	May 99	June 99	Completed
	Final Report	June 99	Oct 99	Completed